BUILDING A MEASUREMENT SETUP FOR THE INVESTIGATION OF ACOUSTIC CAVITATIONS FOR MEDICAL APPLICATIONS

by

Şener Erdem

B.S. in Electrical and Electronic Engineering, Boğaziçi University, 2005

Submitted to the Institute of Biomedical Engineering
in partial fulfillment of the requirements
for the degree of
Master of Science
in
Biomedical Engineering

Boğaziçi University
June 2007

BUILDING A MEASUREMENT SETUP FOR THE INVESTIGATION OF ACOUSTIC CAVITATIONS FOR MEDICAL APPLICATIONS

APPROVED BY:

Assist. Prof. Dr. Burak GÜÇLÜ (Thesis Supervisor)	……...
Assist. Prof. Dr. Ata AKIN	……...
Prof. Dr. Yasemin KAHYA	……...

DATE OF APPROVAL: 12.06.2007

ACKNOWLEDGMENTS

I am greatly thankful to Assistant Prof. Dr. Burak Guclu, for his supervising and support during my thesis work.

I also thank Associate Prof. Dr. Yasemin Kahya and Assistant Prof. Dr. Ata Akin for their patience, support, and valuable comments during my thesis defense.

Finally, I would like to thank all Philips Research, Biomolecular Engineering Department members for their inspiration, support, motivation, and logistical supply during my thesis.

ABSTRACT

BUILDING A MEASUREMENT SETUP FOR THE INVESTIGATION OF ACOUSTIC CAVITATIONS FOR MEDICAL APPLICATIONS

Various noninvasive medical treatments rely on high intensity ultrasound or shock waves. The externally generated pressure waves transfer a large amount of energy into the body. There is evidence that in all of these treatments cavitation provides the main contribution to the desired effects. Cavitation consists of the formation and violent collapse of gas bubbles with sudden gas release. Examples of medical treatments where cavitation plays an important role are the destruction of urinary calculi by application of extracorporeal shock waves, the noninvasive ablation of tumors, localized drug delivery, and improved drug uptake by tissues. Unfortunately, the energy transfer during cavitation is often poorly controlled, frequently leading to inefficient treatment, hemorrhage, and undesired cell damage.

In this study a setup is designed, built and tested to investigate microbubble cavitation and its possible effects on kidney stone destruction in combination with high intensity focused ultrasound (HIFU). Optical cavitation detection is monitored during ultrasound excitation by means of a digital camera. Active and passive cavitation detection techniques are used to detect cavitation events. Micro bubbles with different shell types and size distributions are tested. Artificial kidney stones are tested to see whether the HIFU transducer is able to damage a kidney stone. Preliminary results do not show, however, a significant influence of microbubble infusion on kidney stone destruction by means of HIFU.

Keywords: ultrasound; cavitation; microbubbles; lithotripsy; HIFU

ÖZET

MEDİKAL UYGULAMALAR İÇİN MİKROKABARCIKLARIN KAVİTASYON ÖLÇÜMÜNÜ YAPAN DÜZENEK GELİŞTİRİLMESİ

Çeşitli noninvazif tıbbi tedaviler yüksek yoğunluklu ultrason veya şok dalgalarına dayanır. Harici olarak oluşturulan basınç dalgaları vücut içine büyük miktarda enerji transfer eder. Bu tür tedavilerde istenilen etkilerin oluşumuna kavitasyonun sebep olduğuna dair kanıtlar bulunmaktadır. Kavitasyon, gaz kabarcıklarının oluşup aniden şiddetli olarak çökmesi sonucu kabarcıkların içindeki gazın dışarıya verilmesi olayıdır. Kavitasyon olayının önemli rol oynadığı tıbbi tedaviler arasında ekstrakorporeal şok dalgaları ile böbrek taşlarının kırılması, tümörlerin noninvazif olarak ısıtılması, bölgesel ilaç verilmesi ve verilen ilacın dokular tarafından daha etkin bir şekilde alınması gelmektedir. Maalesef kavitasyon oluşumu sırasında vücuda verilen enerjinin kontrolü çok güç olup, genellikle etkisiz tedavi, iç kanama ve istenmeyen doku zedelenmelerine sebep olmaktadır.

Bu çalışmada, mikrokabarcık kavitasyonunun oluşumunu ve kavitasyonun yüksek yoğunluklu odaklanmış ultrason (HIFU) altında böbrek taşları üzerinde olası etkilerini gözlemleyebilmek için bir ölçüm düzeneğinin dizaynı, geliştirilmesi ve test edilmesi gerçekleştirilmiştir. Ultrasonifikasyon sırasında optik kavitasyon ölçümü dijital bir kamera araciliği ile gerçekleştirilmiştir ve aktif ve pasif kavitasyon yöntemleri kullanılarak kavitasyonun oluşumu gözlemlenmiştir. Değişik mikrokabarcıkların kavitasyon özellikleri test edilmiş ve böbrek taşlarının HIFU altında gerçekleştirilen kavitasyonla kırılıp kırılmadığı yapay böbrek taşları kullanılarak denenmiştir. İlk ölçümlerin sonuçlarına göre kavitasyonun HIFU altında böbrek taşlarının kırılması üzerinde önemli bir etkiye sahip olmadığı görülmüştür.

Anahtar Sözcükler: ultrason; kavitasyon; mikrokabarcıklar; litortipsi, HIFU

TABLE OF CONTENTS

LIST OF FIGURES

LIST OF ABBREVIATIONS

US	Ultrasound
HIFU	High Intensity focused Ultrasound
ACD	Active Cavitation Detection
PCD	Passive Cavitation Detection
PLA	Poly-Lactite-Acid
PVA	Poly-Vinyl-Alcohol
PEG	Poly-Ethylene-Glycol

1. INTRODUCTION

Ultrasound is one of the most widely used medical diagnostic imaging modalities. Ultrasound systems provide real time information about organs, tissues, and blood flow. Apart from diagnostics, ultrasound also foreshadows important therapeutic applications. High intensity ultrasonic waves allow transferring substantial quantities of energy through a medium. When this energy is focused on a small volume, the acoustic intensity is such that the structure of the medium can be modified. A well known example of this modification is the formation of cavitation bubbles due to mechanical forces. In this context, cavitation is defined as a violent bubble collapse with a consequent sudden gas release. Cavitation bubbles can concentrate a large amount of energy and release it in the form of powerful micro-jets while collapsing [1]. Cavitation phenomena are also related to local temperature increases to thousands of Kelvin with resulting light emission [2]. Due to the very high and localized concentration of energy, cavitation is a powerful phenomenon. Therefore, controlling cavitation is very important.

There is mounting evidence that cavitation phenomena are at the basis of a number of medical treatments, such as tumor ablation (heat) and thrombi dissolution by high intensity focused ultrasound, or destruction of urinary calculi (e.g. renal stones) by shock wave (lithotripsy) [3, 4, 7]. Some studies indeed suggest that the stone destruction is a consequence of cavitation rather than of tensile and shear stress induced in the stone by the shock wave gradients [3-6].

A successful use of cavitation in medicine requires reliable means to control it. An understanding of cavitation formation and control is essential. As cavitation is such a violent phenomenon, tissue damage can easily occur. Therefore, an increased control on cavitation can result in safer applications.

Against this background, many parameters have been investigated to control the incidence of cavitation phenomena: the fluid viscosity, the static pressure, the compressive and rarefactional wave pressure, the ultrasonic pulse (or shock wave) shape and frequency components, as well as their repetition frequency [1, 8-11]. Several methods, mainly involving ultrasound techniques, have been employed to quantify cavitation. Two main ultrasound methods exist: active and passive cavitation detection (ACD and PCD, respectively) [12-15]. In ACD, cavitation is detected from the backscatter of transmitted pulses. In PCD, the spectrum of the signal generated by cavitation bubbles is analyzed. However, these methods only permit to detect the occurrence of cavitation. No method is presently developed to quantify cavitation activity [16].

The addition of cavitation agents, instead of relying on cavitation to take place naturally, can in principle control the transfer of energy related to cavitation, allowing for the minimization of side effects and optimization of cavitation efficiency. A recent development of ultrasound diagnostics is the introduction of ultrasound contrast agents (UCAs). UCAs are administered intravenously, resulting in an increasing reflection of ultrasound by the blood pool. UCAs are microbubbles made of an inert gas encapsulated in a shell of a biocompatible material, which scatter ultrasound very efficiently [17, 18]. The combined use of microbubbles and ultrasound should not be limited to diagnostic imaging, as it also offers important new opportunities for medical treatments. UCAs are examples of artificial cavitation agents and they have shown significant enhancement of cavitation phenomena [9, 19].

Promising medical treatments are, for instance, tumor ablation [19, 22, 23], and localized drug delivery [24, 25]. In the latter, bubbles are used as cavitation agents to induce an increased permeability of the cell membrane and consequently increase drug uptake [26-28]. Hynynen [29] has shown the applicability of these techniques also for drug delivery through the blood brain barrier. Another application where the use of microbubbles has been considered is thrombolysis [25, 30]. The use of ultrasound and microbubbles for these applications allows for a much localized minimally invasive treatment and is therefore likely to cause fewer side effects. The presence of microbubbles not only lowers the energy levels

that are necessary to produce cavitation, but also changes the acoustic properties of the medium and the relation between cavitation and its control parameters [21, 28].

Despite the potential applications, research on cavitation characterization is still very limited and focused only on single bubble modeling. A quantitative characterization of cavitation in the presence of multiple bubbles and the macroscopic model of cavitation formation, control, and effects on its surroundings do not exist. The latter is in fact the fundamental knowledge that is necessary to exploit cavitation phenomena for efficient and optimized noninvasive medical applications, which are safer and more effective. In particular, the ratio between desired (destruction or treatment of selected targets) and undesired (damage to healthy tissue) effects must be maximized.

1.1 Aim of the Thesis

In this thesis, a setup is built in which the cavitation of the agents are measured and studied. An energy (pressure) source is used to induce cavitation and the effects are followed using different sensors. Ultrasonic, electronic, and optical sensors are adopted and interchanged for the analysis. A cavitation agent detection system (B-mode ultrasound) is used to detect the agent distribution and optimize the timing of the high pressure pulses. Newly designed signal processing techniques are introduced.

2. BACKGROUND

This chapter is organized as follows: Section 2.1 introduces brief information about the physics of ultrasound. In Section 2.2, microbubbles and their potential use in medical applications are explained. In section 2.3, brief information about cavitation and its effects are stated.

2.1 Physics of Ultrasound

Just as audio sound is the transmission of pressure waves through a medium such as air or water, ultrasound is the same type of transmission of pressure waves, but at frequencies above human hearing, or above 20,000 Hz. As with light waves, these ultrasonic waves can be reflected, refracted, focused, and absorbed. Unlike light waves, ultrasonic waves are very physical in nature; they are actual movement of molecules as the medium is compressed (at high pressure) and expanded (at low pressure), and thus ultrasound can act physically upon biomolecules and cells. Most importantly, unlike visible light waves, ultrasonic waves are absorbed relatively little by water, flesh and other tissues. Therefore, ultrasound can see into the body and can be used to transmit energy into the body at precise locations.

2.1.1 Uses of Ultrasound

The traditional use of ultrasound in medicine is for diagnostic imaging (which occurs at low average intensities and high frequencies) and for tissue heating (which occurs at higher intensities and higher frequencies). The intensity of an ultrasonic beam is measured in terms of power carried per cross section area of the beam, typically having units of Watts/cm^2. If a beam is focused down to a small size on a target tissue, the power per area becomes very large and significant thermal energy can be absorbed from the beam by the tissue, resulting in heating. Such hyperthermia has been traditionally employed in physical therapy to warm

tissues [31], in drug delivery to melt drug-containing liposomes [32], and in medical therapy to kill or ablate tissue [33–35]. Thus hyperthermia in targeted drug delivery accomplishes the role of heating the drugs, drug carriers, and the tissues receiving the drugs.

2.1.2 Contrast Enhanced Ultrasound

Contrast-enhanced ultrasound is the application of ultrasound contrast agents to traditional medical sonography. Ultrasound contrast agents are gas-filled microbubbles that are administered intravenously to the systemic circulation. Microbubbles have a high degree of echogenicity, which is the ability of an object to reflect the ultrasound waves. The echogenicity difference between the gas in the microbubbles and the soft tissue surroundings of the body is immense. Thus, ultrasonic imaging using microbubble contrast agents enhances the ultrasound backscatter, or reflection of the ultrasound waves, to produce a unique sonogram with increased contrast due to the high echogenicity difference. Contrast-enhanced ultrasound can be used to image blood perfusion in organs, measure blood flow rate in the heart and other organs, and has other applications as well.

Targeting ligands that bind to receptor characteristic of intravascular diseases can be conjugated to microbubbles, enabling the microbubble complex to accumulate selectively in areas of interest, such as diseased or abnormal tissues. This form of molecular imaging, known as targeted contrast-enhanced ultrasound, will only generate a strong ultrasound signal if targeted microbubbles bind in the area of interest. Targeted contrast-enhanced ultrasound can potentially have many applications in both medical diagnostics and medical therapeutics.

2.2 Microbubbles

An ultrasound contrast agent is made of tiny microbubbles, which scatter ultrasound very effectively. The bubbles consist of air or an inert gas and they are coated with a protein,

lipid or polymer layer. This prevents the bubbles to either dissolve in the blood or to coalesce to form larger bubbles. The contrast agents are injected in the patient's arm and they are so small that they are transported into the smallest capillaries. Using contrast enhanced echocardiography the cardiologist can see which part of the heart muscle is poorly perfused. In Figure 2.1 some microbubbles at different sizes are seen.

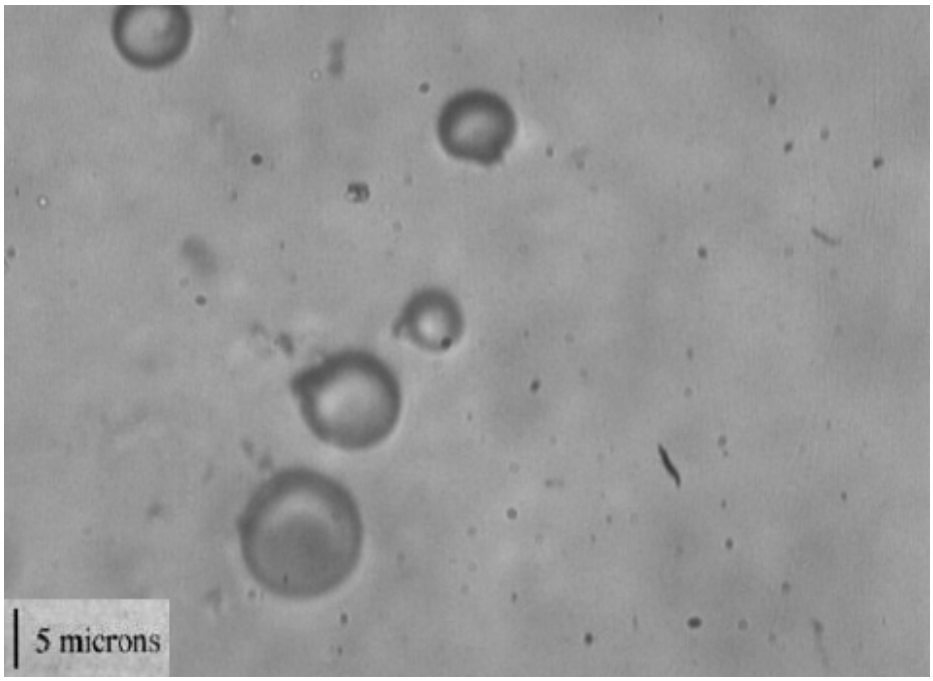

Figure 2.1 Some microbubbles at different sizes produced during the experiments.

The rapidly developing field of contrast enhanced ultrasound relies on the detection of gas-filled, encapsulated microbubbles that produce a unique signature in an acoustic field. These microbubbles behave similarly to red blood cells in the microcirculation, and have been used to enhance the blood pool and assess tissue blood flow at the microvascular level. Perfusion imaging with contrast enhanced ultrasound uniquely provides information on capillary blood volume and the capillary blood velocity. Accordingly, this technique has recently been used to study how abnormal capillary responses contribute to diseases such as coronary artery disease and hyperlipidaemia, and whether these abnormalities can be modulated by drug therapy. Another very promising future application is the development of

site-targeted microbubble contrast agents that can be used to image molecular events *in vivo*. These agents have been used to non-invasively assess inflammation, angiogenesis and early tumor formation. Potential uses for targeted contrast-enhanced ultrasound extend beyond diagnostic applications. It can be used to rapidly assess new therapeutic strategies aimed at modulating the targeted molecular mediators. Moreover, there is now evidence that contrast ultrasound can be used to deliver therapeutic agents such as plasmid DNA and drug directly to tissue by ultrasound-mediated destruction of payload-bearing microbubbles. The ability to target these microbubble agents to molecular markers of disease, together with the use of focused ultrasound imaging, holds great promise for the localization of drug/gene delivery.

2.3 Cavitation

Cavitation is the formation and/or activity of gas-filled bubbles in a medium exposed to ultrasound [36]. As the pressure wave passes through the media, gas bubbles of any size will expand at low pressure and contract at high pressure. If the resulting oscillation in bubble size is fairly stable, the cavitation is called stable or non-inertial cavitation. Such oscillation creates a circulating fluid flow around the bubble [37–39] with velocities and shear rates proportional to the amplitude of the oscillation. At high amplitudes the associated shear forces are capable of shearing open red cells and synthetic vesicles such as liposomes [40].

As the ultrasonic intensity increases, the amplitude of oscillation also increases to a point in which the inward moving wall of fluid has sufficient inertia that it cannot reverse direction when the acoustic pressure reverses, but continues to compress the gas in the bubble to a very small volume, creating extremely high pressures and temperatures [41, 42]. This type of cavitation, called transient, inertial or collapse cavitation can be detrimental to cells or vesicles because of the very high shear stresses in the region of the collapse, the shock wave produced by the collapse, and the free radicals produced by the high temperatures. The collapsed bubble often fragments into smaller bubbles that serve as cavitation nuclei, grow in size, and eventually collapse again [41, 42]. Figure 2.2 shows a streak optical photograph

before, during and after a cavitation collapse [42]. On the left is the original microbubble. The middle frame is a high speed streak photograph showing the boundaries of the bubble when subjected to ultrasonic pressure; the pressure measurement is recorded at the top of the photograph. The right frame shows the resulting fragments of the bubble. Cavitation is a violent phenomenon that concentrates the energy from ultrasound into a small volume.

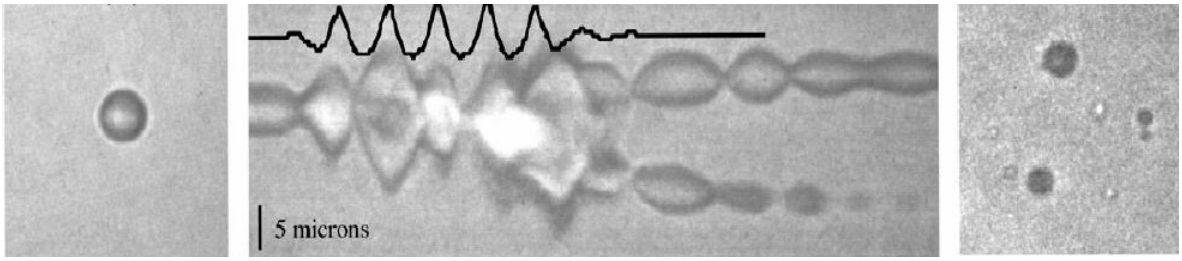

Figure 2.2 Optical images of a 2.5 μm-radius microbubble exposed to ultrasound [2].

Furthermore, if the collapse is near a solid surface, an asymmetrical collapse occurs which ejects a liquid jet at sonic speed toward the surface [41]. Figure 2.3 illustrates this type of collapse. If the rigid surface is a blood vessel wall, skin, a large cell, or semi-rigid vesicle, then the jet can pierce the surface.

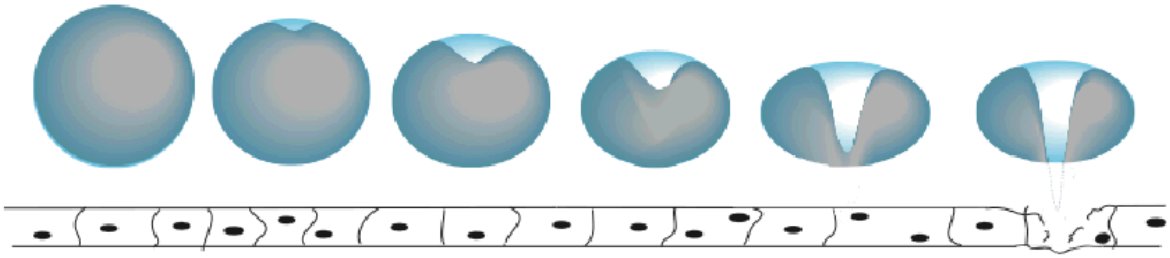

Figure 2.3 Illustration of an asymmetric collapse of a bubble near a surface, producing a jet of liquid toward the surface [2].

Since collapse cavitation can be damaging to biological tissues, there has been much research into the conditions under which it is produced. In general the likelihood and intensity of collapse cavitation increase at higher intensities and lower frequencies, as has been demonstrated by experiments [41, 43, 44] and theory [45]. The size of the bubble and its

physical properties, such as gas species, interfacial tension, and surface rigidity also affect the cavitation process [46–50].

3. METHODS

This chapter briefly introduces the methods used in this study. In Section 3.1, overview of the measurement setup is explained. In section 3.2, the production technique of microbubbles is explained. In section 3.3, design of the flow system for optical visualization of cavitation events is explained. In section 3.4, design of the experimental setup for active and passive cavitation detection is explained.

3.1 Overview of the Setup

The setup that is build is designed in such a way that multiple measurements can be carried out at the same time. Figure 3.1 shows the experimental configuration of the total setup including a digital camera, a microscope, US transducers, an RF amplifier, signal generators and a B-mode US scanner.

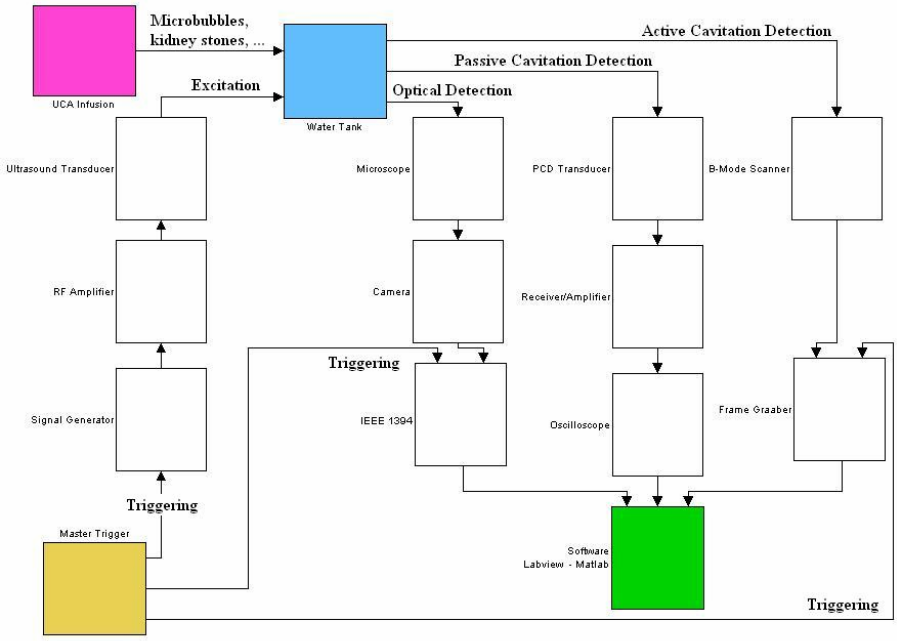

Figure 3.1 Schematic overview of the experimental setup for cavitation measurements.

The purpose of the HIFU transducer is to generate high amplitude sound waves that initiate cavitation events. The focal length of the HIFU transducer is 70 mm. The HIFU transducer is driven by a radio frequency power amplifier (ENI 240L, the Netherlands). The signal driving the amplifier is generated by an arbitrary waveform generator, (Agilent Technologies, Santa Clara, CA, USA). This generator supports both continuous and burst waveforms and it can be externally triggered.

An US transducer (Panametrics, Waltham, MA, USA) is used for PCD. This transducer has a broadband response and it is therefore suitable for receiving signals over a broad frequency spectrum. The US transducer has sufficient sensitivity on the frequency range of interest to detect the broad spectrum that is generated by cavitation events. To amplify the signal generated by the US transducer, a pulser-receiver (Panametrics, Waltham, MA, USA) is used. The amplified signal is displayed on an oscilloscope (Agilent Technologies, Santa Clara, CA, USA). The oscilloscope is connected to a PC (Pentium 4 2.8 GHz, 512 MB RAM). The data obtained by the PC is stored for further post-processing.

ACD is performed by an ultrasound scanner (Advanced Technologies Laboratories, Germantown, MD, USA). The scanner supports the adjustment of several parameters like the sector angle, depth, output power and gain. The images made by the scanner are transferred to a PC by means of a frame grabber (National Instruments, Austin, TX, USA). The data obtained by the frame grabber is then processed by LabView (National Instruments, Austin, TX, USA).

Optical cavitation detection is recorded by means of a digital camera (Allied Vision Technologies, Germany). The digital camera is a charge coupled device (CCD) based camera. The purpose of the camera is to make an image in between two consecutive HIFU pulses. The camera supports adjustment of shutter time and gain to improve image quality. Images are transferred to the PC by means of an IEEE-1394 (firewire) interface. Because the digital camera is combined with a microscope system detailed images can be obtained. The microscope system is a custom built Leica Optical Zoom system (Leica Microsystems, Bannockburn, IL, USA).

3.2 Microbubble Constructs Made Using the Ink – Jetting Technique

A method has been developed to prepare polymeric capsules with an extremely narrow size distribution using drop-by-drop emulsification methods such as ink-jet printing. Every emulsion drop that is prepared has the same size and the emulsion droplets shrink by removal of the solvent yielding particles or capsules. Schematically the process is illustrated in Figure 3.2 below:

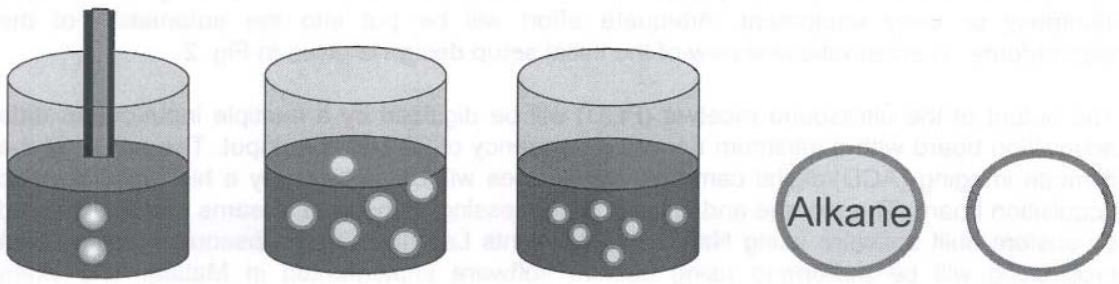

Figure 3.2 The preparation of gas containing capsules with a narrow size distribution.

A solution containing the shell forming material, such as poly-lactide, a good solvent for these materials, such as dichloroethane, and an alkane solution, such as cyclo-octane, is brought into an aqueous poly-vinyl-alcohol (PVA) solution drop by drop. This is done using a piezo driven inkjet nozzle and, therefore, all drops have the same size. The good solvent dissolves into the aqueous phase and is evaporated or extracted. The shell forming material precipitates on the boundary with the solution and only the alkane is left as the core of the capsule. Subsequently the alkane is removed by freeze drying. Some microbubbles produced by this technique and detected by the microscope and digital camera are seen in Figures 3.3 and 3.4 below.

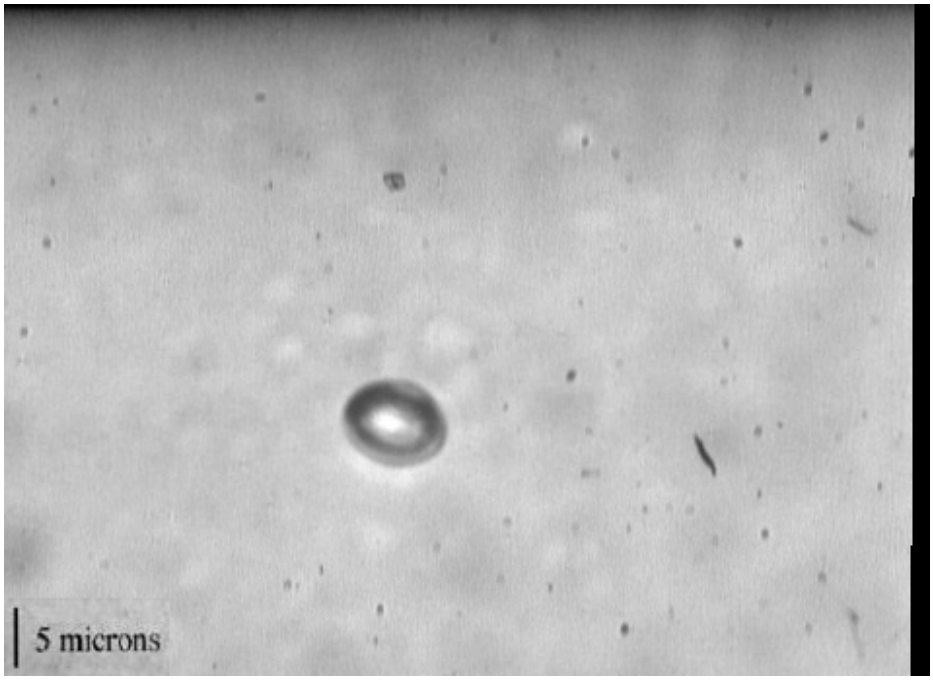

Figure 3.3 A single microbubble produced by our ink-jetting technique.

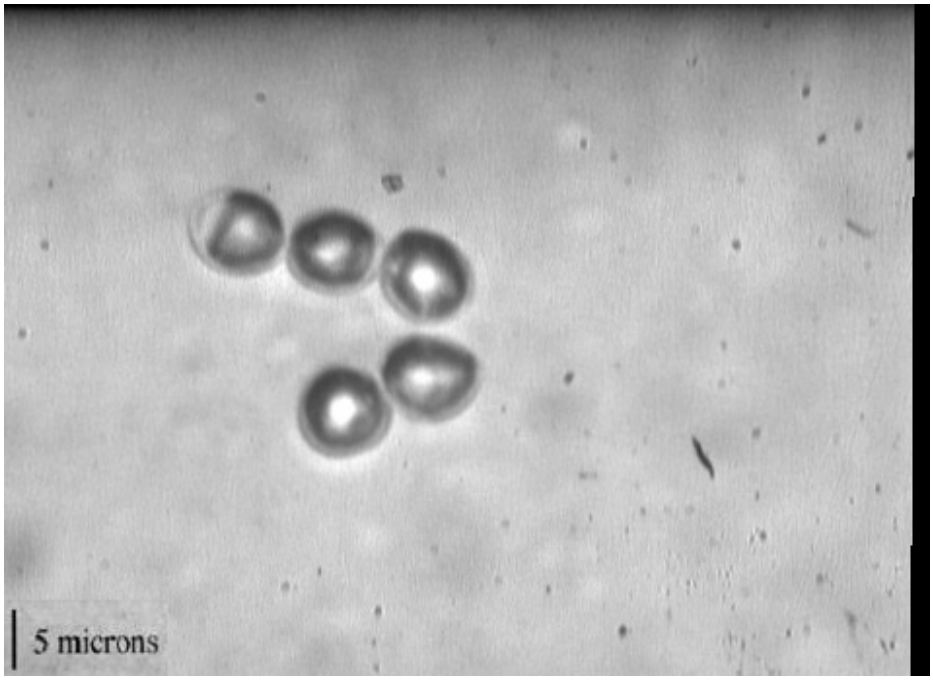

Figure 3.4 Some microbubbles produced by our ink-jetting technique.

This method not only allows for the preparation of monodisparse particles, but also allows for precise tailoring of the comparison of the particles. As all material, except for the solvent, originally present in the emulsion droplet ends up in the particle, the composition of each particle is known exactly. A summary of the final method is presented in the protocols section in Appendix A.

3.3 Design of the Optical Flow System

3.3.1 Material Selection

The acoustic properties of several plastics to use in the flow chamber were characterized. The experimental setup is depicted in Figure 3.5. Transmission was tested at 1MHz, since this is within the range of medical ultrasound scanners. The function generator was used to create 5 cycle bursts at 1 MHz and the received signal was measured. Then, varying materials were placed in the ultrasound path and the signal was measured again.

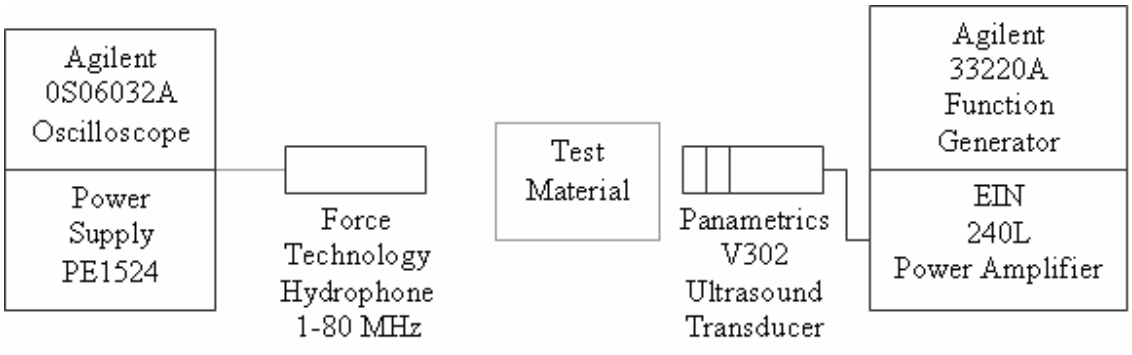

Figure 3.5 Schematic of the setup used to test the acoustic transmission of various materials.

As shown in Figure 3.6, of the materials tested, polystyrene and PMMA had low attenuation coefficients (as shown by the small slope), but polystyrene additionally had the least amount of reflection (as shown by the near zero intercept). The transmission coefficient of polypropylene points to some error in the measurement, likely due to inaccurate estimates

of the material thickness. The polystyrene nevertheless appears to be the superior choice so polystyrene cover slips were obtained.

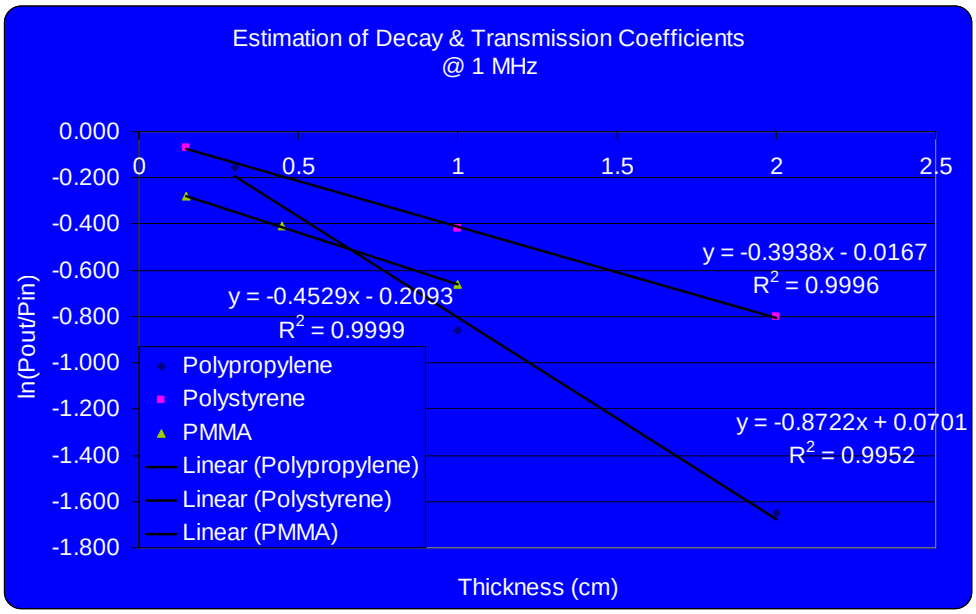

Figure 3.6 Results for acoustic transmission through various plastics.

An additional consideration was how to direct the ultrasound waves once they passed through the flow chamber. Because of the large impedance mismatch between air and water, a plastic selected to couple to the water with minimal reflection would inherently lead to reflection at the air interface. If the flow cell is to be used to look at the effects of acoustic radiation on microbubble transport to the surface, it is important to direct the reflected energy away from the focal region. A scheme was developed so that the acoustic energy reflected into the flow chamber would not re-enter the focal region. The ultrasound transducer was angled 25^{o} from the normal to reflect ultrasound wave away from the focal region and also to allow visualization with transmitted light from below.

A long working distance objective allowed the use of a thick, 1 cm plastic piece atop the flow chamber to give the longitudinal ultrasound wave sufficient distance before re-entering the flow chamber. Although optically clear polystyrene was not available in this

thickness a special, cross-linked, clear polystyrene called Rexolite 1422, marketed for applications in acoustic and optical lenses, was obtained. A schematic of the plate assembly is depicted in Figure 3.7. The mounting should be done while submerged to avoid entrapping air in the gap between the cover slip and grooved plate, which would reflect the ultrasound.

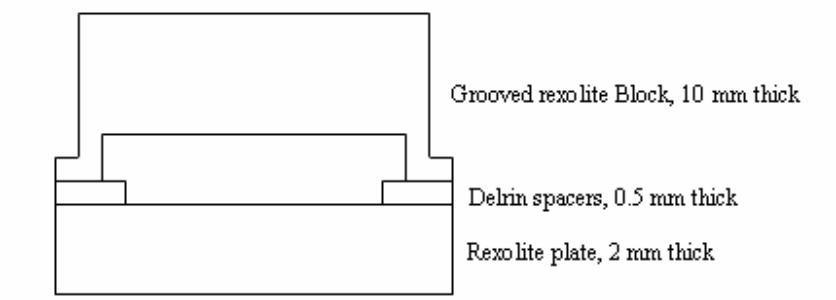

Figure 3.7 Design of the flow cell. A polystyrene cover slip can be inserted in the gap in the grooved rexolite block.

A schematic of the entire setup is shown in Figure 3.8. A metal clip secures the ultrasound transducer to the objective, so the ultrasound and microscope remain confocal as the flow chamber, supported by the water tank, is moved on the XY stage.

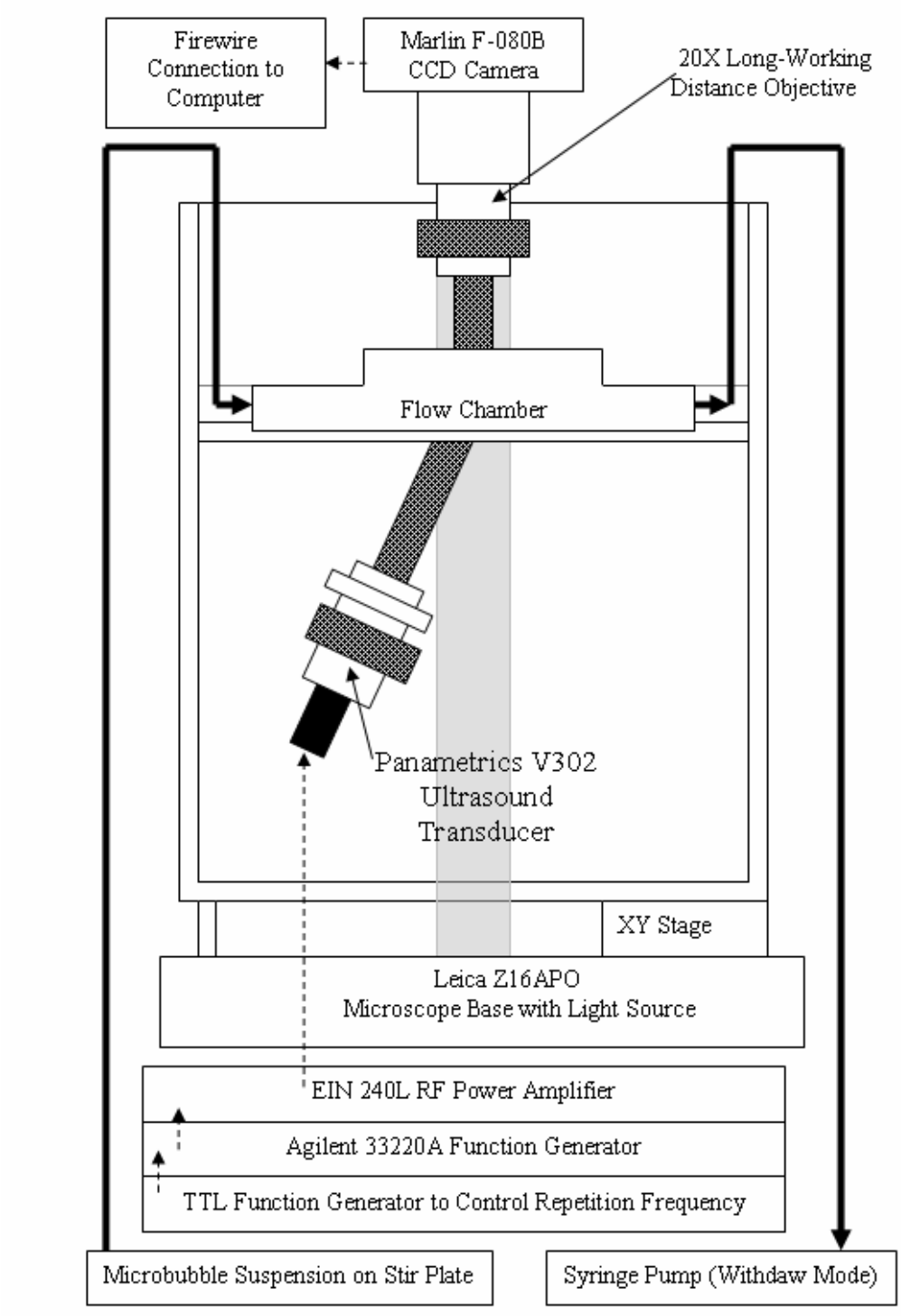

Figure 3.8 Schematic of the flow chamber setup complete with electronics.

Below are shown the pictures of some of the components of the setup. In Figure 3.9, the picture of the flow cell components are shown; in Figure 3.10, the picture of the mounted flow cell to the water tank is seen; and in Figure 3.11, the picture of the entire setup is shown.

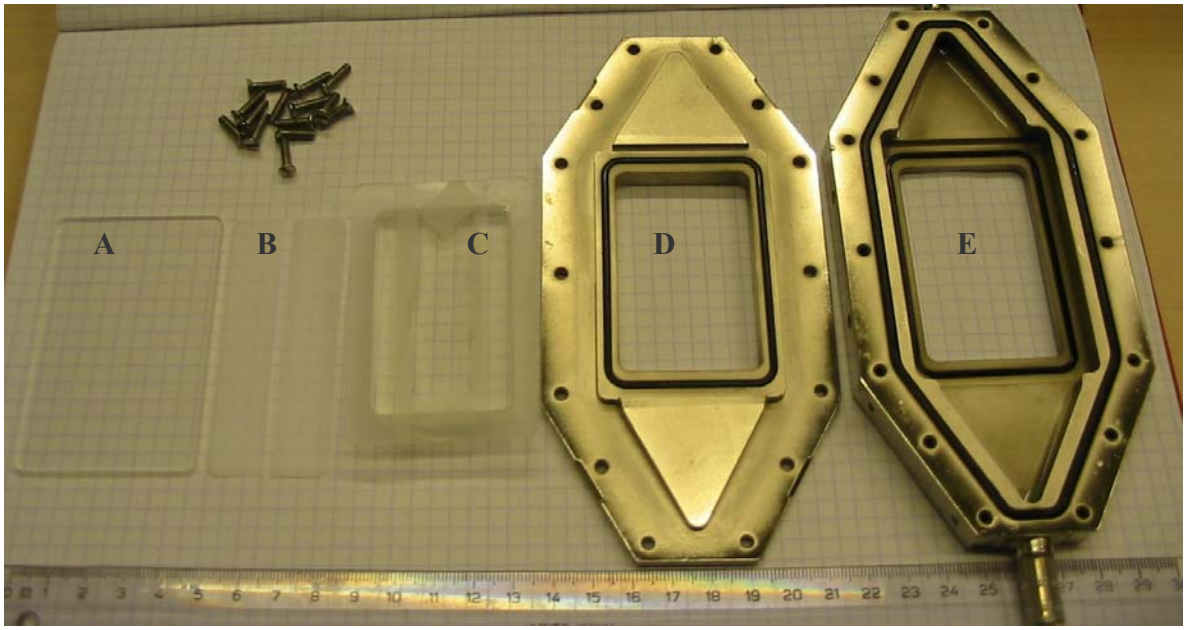

Figure 3.9 Picture of the chamber components. A. The bottom rexolite plate. B. Two delrin spacers. C. Thick rexolite block with groove for the coverslip. D. Bottom flow plate holder. E. Top flow plate holder.

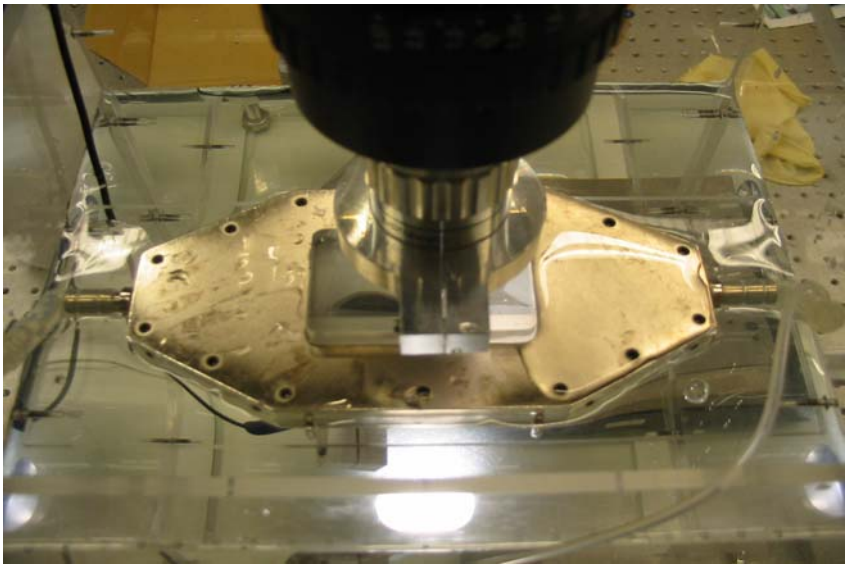

Figure 3.10 Picture of the mounted flow chamber.

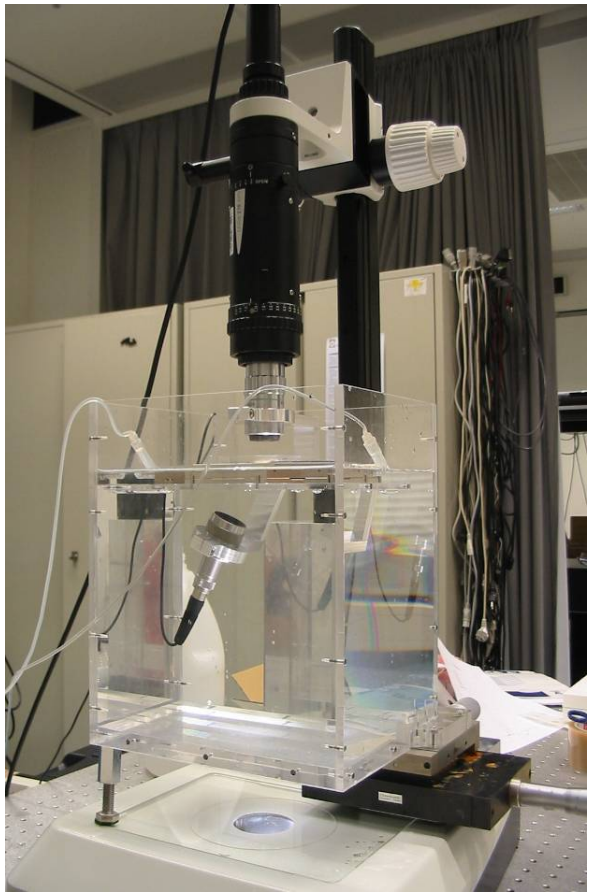

Figure 3.11 Picture of the microscope setup with the flow chamber and ultrasound transducer.

3.3.2 Microbubble Infusion

The infusion of the microbubbles to the specified target is obtained by a stir plate and syringe pump setup. If the flow rate is set to 5 mL/min, with a 50 mL syringe pump, it is possible to maintain flow for 10 minutes. The linear rate of the syringe pump appears to be high enough so syringe sticking does not lead to pulsatile flow. The available syringes are estimated to have a diameter of 2.9 cm. In Figure 3.12, the syringe pump and stir plate are shown. The stir plate ensures the bubble samples are mixed. The syringe pump is operated in withdraw mode.

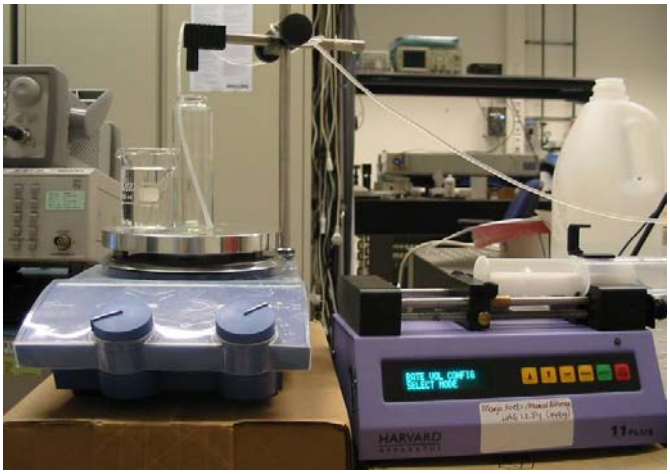

Figure 3.12 The syringe pump and stir plate. The stir plate ensures the bubble samples are mixed. The syringe pump is operated in withdraw mode.

3.4 Design of the Active and Passive Cavitation Detection Setup

3.4.1 Water Container

The water container is the core of the setup. All devices and parts are located in or connected to this container. The side walls and bottom of the tank are made of PMMA. PMMA matches acoustically well with water so that the amount of reflections at the water-wall interface is limited. Sound waves that are transmitted through the water-wall interface reflect on the wall-air interface. A possibility to reduce these unwanted reflections is to install acoustic absorbers inside the tank. A disadvantage of these absorbers is that they limit light in the water container. Another solution to decrease the reflected energy consists of increasing the thickness of the walls. By increasing the thickness of the walls more energy is absorbed and the sound wave that is reflected at the wall-air interface is limited in amplitude. The most reflections occur at the water-air interface at the top of the water container. These reflections can be limited by fixing a sponge in the water. Figure 3.13 gives a schematic overview of the water container and the connected transducers.

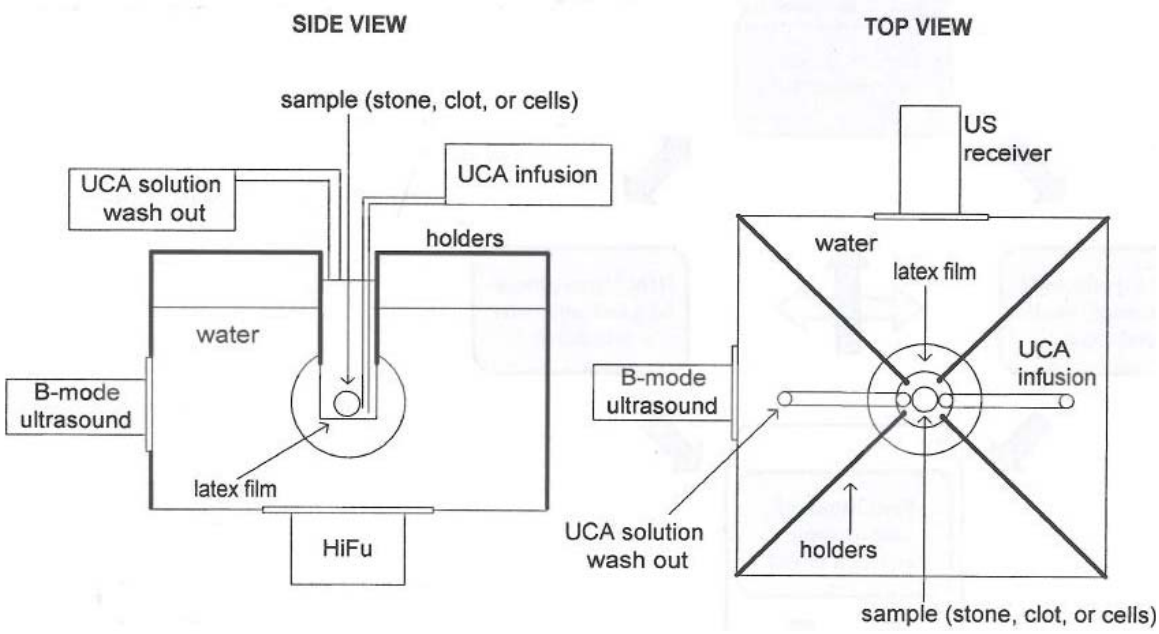

Figure 3.13 Schematic of the ACD and PCD setup.

The HIFU transducer is fixed on the bottom of the tank. This transducer is placed in a PMMA holder to overcome leakage. The transducer used for PCD is fixed into a side wall with the same construction as the HIFU transducer. The ACD transducer, which has a different form, is fixed directly into the side wall perpendicular to the PCD transducer to limit the interaction between the transducers. An acoustically and optically transparent holder, Rexolite 1422, is fixed on the bottom of the tank. The holder is fixed in a way that a kidney stone can be placed exactly above the HIFU transducer at a distance that is equal to the focal distance of the transducer. In figure 3.14 the kidney stone holder is seen and the plastic tube that infuses the micro bubbles into the focal region is also visible. This tube is embedded in the holder to keep it on a fixed position during the experiments.

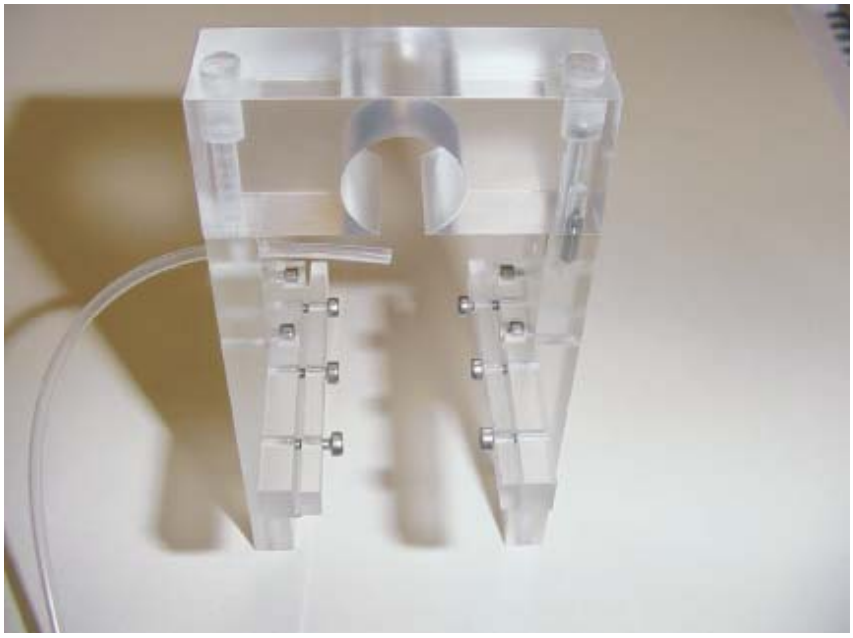

Figure 3.14 Kidney stone holder.

In Figure 3.15 and in Figure 3.16, the HIFU transducer and the B-mode ultrasound scanner are seen, respectively.

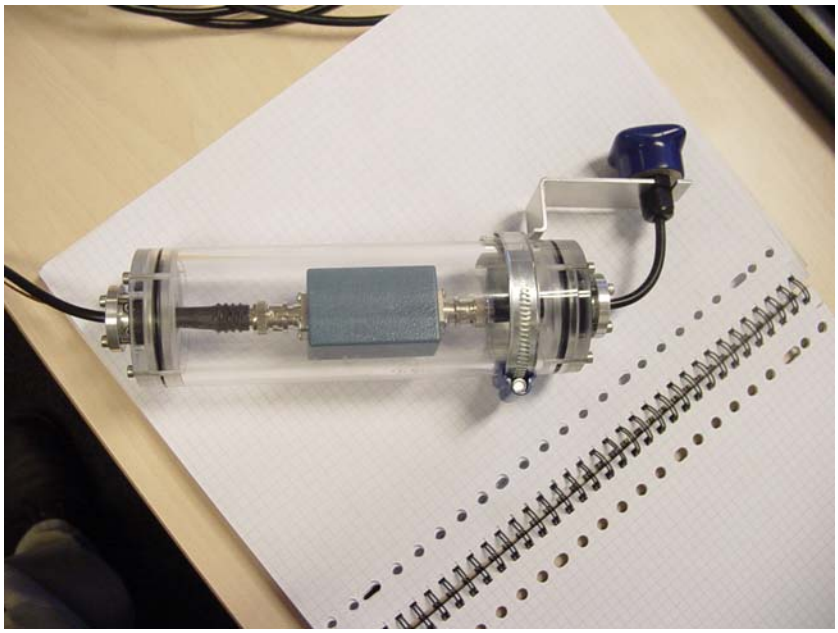

Figure 3.15 HIFU transducer

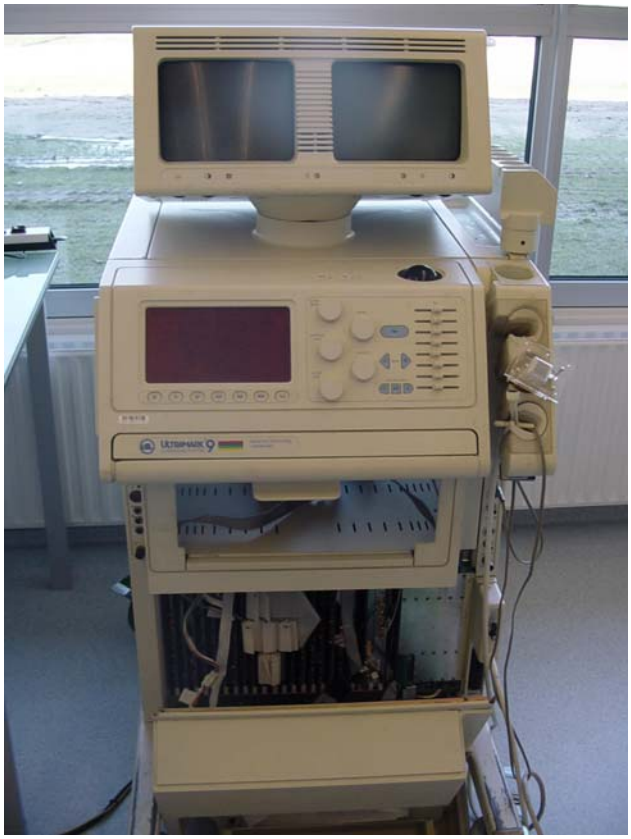

Figure 3.16 B-Mode ultrasound scanner

3.4.2 Synchronization

During the experiments a large amount of data is generated. The images of both the digital camera and the B-mode US scanner are transferred and stored in a PC. The signal received by the scope is transferred to the PC and saved. After the experiment the data should be available for off-line processing. In order to ensure that all the data is collected in the time period between two consecutive HIFU pulses, the acquisition system must be properly synchronized. Every sensor has a different time window of interest, so that synchronization is complicated and additional trigger signals and delays are needed.

The data (digital image, US image, and PCD data) that is generated during an experiment is stored in clusters. Every cluster is linked with the number of the generated HIFU

pulse and is sorted out. For instance, the Nth cluster contains the images and the PCD data that are recorded after the Nth HIFU pulse excitation. The length in between two consecutive HIFU pulses is determined by the pulse repetition frequency (PRF). The PRF is currently limited by the infusion of the microbubbles. Microbubbles need time to reach the focal zone of the HIFU transducer in large numbers. Earlier research showed that high infusion rates increase cavitation activity and decrease the damage threshold for tissue ablation [53]. Therefore, a relative high infusion rate of 5 mL/min with a concentration of 1 million microbubbles per mL is chosen.

Another property that strongly affects the experiments is the number of cycles of a HIFU pulse. Ammi et al. proved that increasing the number of cycles decreased the needed peak rarefactional pressure to cause cavitation [51]. The pulse length, however, is limited because of two reasons. As already said, the micro bubbles need time to reach the focal region in large numbers. Continuous excitation would prevent this because the bubbles are drifted away by radiation force from the focal zone of the HIFU transducer [55]. The second reason is the time that is needed to transfer and save the PCD data. Because of the high sample rate, a large amount of data is generated. This data should be transferred and saved before the next excitation. A long pulse length decreases the time that is available to transfer and save the data assuming a fixed PRF.

All devices are triggered by a master trigger signal generated by a signal generator. The frequency is equal to the PRF. All three sensors have different time windows of interest. Figure 3.17 presents the time windows of interest for the digital camera and the active and passive cavitation detection transducers. Figure 3.17a shows the HIFU signal and the initial and rebound collapses of the micro bubbles. The PCD transducer (Figure 3.17b) records the backscatter from the HIFU pulse, the first cavitation event, and rebound collapses. The time duration of these events is approximately 5 μs, assuming short pulse duration [51]. The acquisition interval of the oscilloscope is established at 10 μs to ensure that no information is lost. The delay between the start of the HIFU excitation and the start of the time window can be derived given the distance the pressure waves have to travel and their velocity in water. The travel distance is equal to the focal lengths of the HIFU and the PCD transducer: 70 mm + 45

mm = 115 mm. With a speed of sound in water of approximately 1500 m/s this results in a travel time of 76,56 µs.

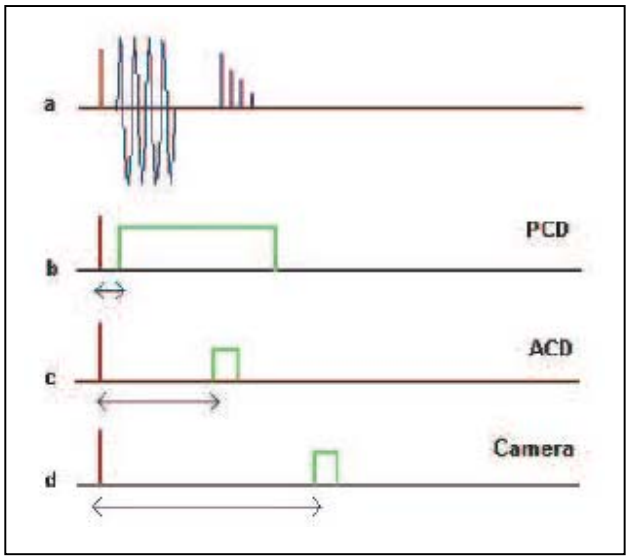

Figure 3.17 Time windows of interest of different sensors.

The ACD transducer, Figure 3.17c, records the collapse caused by the initial cavitation of the gas released from a cracked bubble. Triggering of the US scanner is very critical because the scan time of a single image is long compared to the collapse time. Because this time is much longer than the travel time of the pressure waves from the HIFU transducer to the focal zone, the US scanner is triggered before all the other devices. This is done by adding a delay between the master trigger signal and all the connected devices, excluding the US scanner. This delay should be at least equal to 5 ms because the distance from both the HIFU transducer and the transducer of the US scanner is equal to 70 mm. The acquisition moment of the digital camera, Figure 3.17d, is not very critical. The only condition that has to be met is that an image is required between 2 consecutive HIFU pulses.

3.4.3 Software Implementation

All the data generated during an experiment is displayed, saved and processed by means of custom written software. For transferring, displaying and saving the data on a PC, LabView 7.1 (National Instruments, Austin, TX, USA) is used. Post-processing applications are performed in Matlab 7.14 (The MathWorks, Natick, MA, USA). During the experiments graphical presentations of all generated data should be available. In this way, cavitation events and possible damages on the kidney stone can be monitored in real-time.

A program is written to process both the image of the digital camera and the image made by the US scanner. The program is structured in a sequential way, where the states are executed in a fixed order. After the program leaves the idle state a queue is filled with the tasks to be executed. In the first state the program initializes the connections between PC, digital camera and frame grabber. After initialization, the program moves to the next state, in which it waits for the master trigger signal. When the master signal is detected, the last recorded images of the digital camera and the US scanner are transferred to the PC. Directly after the images are loaded into the LabView program, they are saved as an AVI movie. The videos from the digital camera and the US scanner are saved in series because simultaneous writing of two AVI files on the same hard drive slows down the program. If the multiple acquisition button is pressed, the program comes into a loop where states are iteratively executed. If the stop button is pressed or the program does not receive a trigger signal for 10 seconds, the program is terminated.

In parallel to the image acquisition, another program is executed to process the data generated by PCD. The program, similarly to the image acquisition program, is structured in a sequential way. In the first state the connection with the scope is initialized and the trigger settings of the scope are adjusted. After the master trigger signal is detected, the scope samples a time window of a fixed length and this data is transferred to the PC and displayed on the LabView front panel. The data is saved to the hard drive by means of the transfer data management (TDM) protocol. The TDM protocol, which is a standard feature of LabView 7.1, saves the data in a fast and efficient way. Without this protocol it is not possible to save the

data during the experiment. Saving after the experiment is very time consuming and, therefore, not preferred. When the data is saved and the program is in the multiple excitation mode, the program goes to the state where it waits for the next master trigger signal. The software to perform post-processing analysis is written in Matlab. The frequency content of the PCD signal is analyzed by a fast Fourier transform.

3.4.4 Kidney Stones

The experiments are performed with artificial kidney stones with different densities, sizes and compositions. The first type of stone tested was made of brushite (CaHPO4.2H2O). Brushite is a mineral that was considered as the best among other materials for kidney stone modeling [56]. An artificial kidney stone is seen in Figure 3.18.

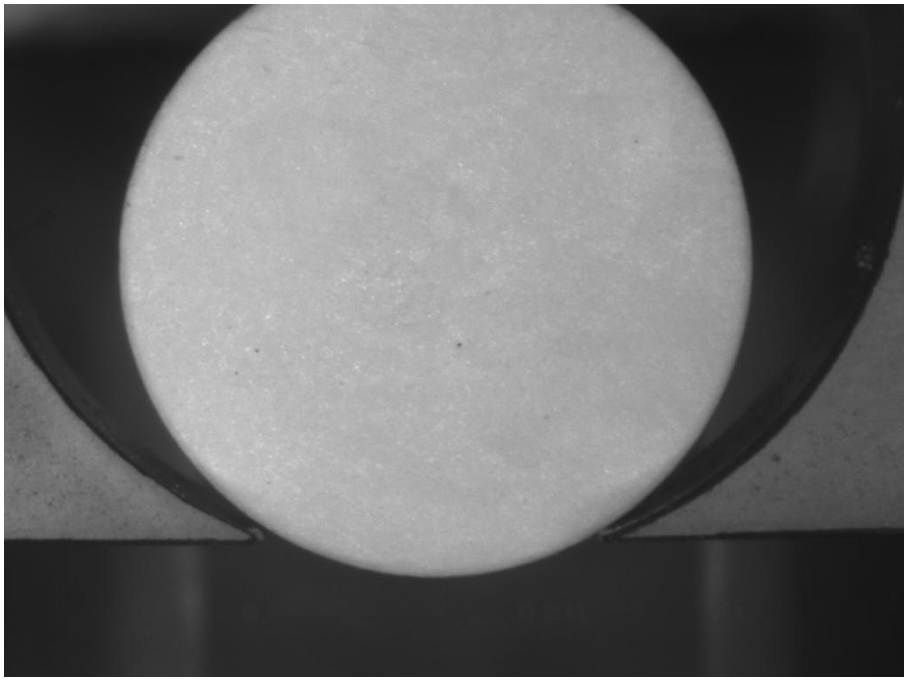

Figure 3.18 Artificial kidney stone in holder during an experiment.

Other smaller stones made of plaster were also tested. Plaster is often used as a mimicking material for kidney stones because it is a good model for small and soft stones

[56]. The weights of the kidney stones are measured before and after the experiment to quantify material loss.

4. CALIBRATION MEASUREMENTS

Before the final experiments were performed, some calibration experiments were done to check whether the single components of the setup worked and if there was any interaction between the different devices that could disturb the measurements. In chapter 4.1, the interactions between the HIFU transducer and the PCD transducer are given. In chapter 4.2, the interactions between the HIFU transducer and the ultrasound scanner are given. In chapter 4.3, the interactions between the PCD transducer and the ultrasound scanner are given. Finally in chapter 4.4, some other calibration measurements are explained.

4.1 Interaction between the HIFU Transducer and the PCD Transducer

The first possible interaction could be between the HIFU transducer and the PCD transducer. The PCD transducer is used to detect scattered signals due to the presence of microbubbles in the focal zone. It should be prevented that sound waves transmitted by the HIFU transducer reach the PCD directly.

To check if an interaction was present, a test experiment was performed. The HIFU transducer was driven at its resonance frequency, between 10 and 90 % of its maximum power, by a continuous sinusoidal signal. The measured output of the amplified signal recorded by the PCD transducer did not show any power content in the region near 8 MHz higher than the noise level. We could therefore conclude that no perceptible interaction between these two devices was present.

4.2 Interaction between the HIFU Transducer and the US Scanner

Another possible interaction could be between the HIFU transducer and the US scanner. When both devices were driven simultaneously, the image of the US scanner was disturbed by the sound waves transmitted by the HIFU transducer. Figure 4.1 shows the interaction between the HIFU transducer and the ultrasound scanner. The relatively whiter sector in the middle is due to the HIFU transducer.

It has to be prevented that the interaction disturbs the region where the kidney stone and the microbubbles are located during the experiment. This can be done by limiting the length of the HIFU pulse or by interrupting the direct path between both transducers. When longer pulse lengths were used a sponge was used to interrupt the direct path between the transducers.

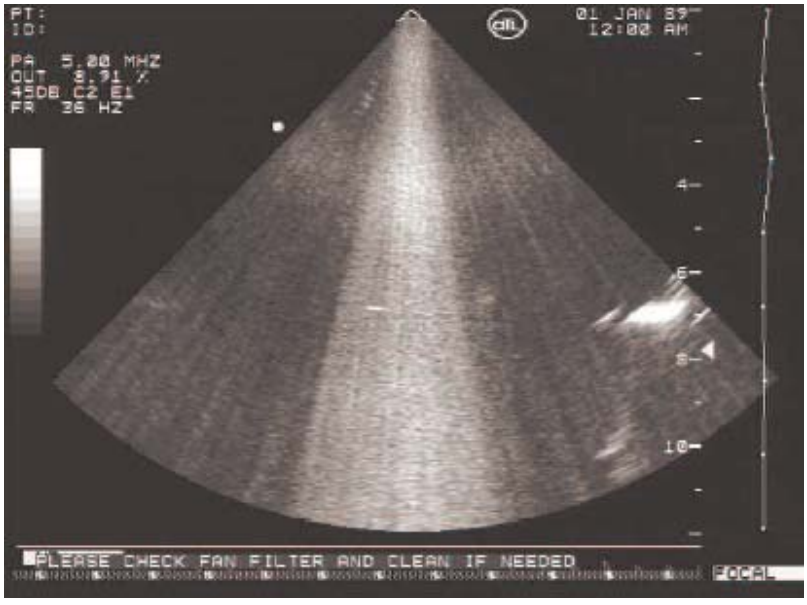

Figure 4.1 Visualization of the interaction between the HIFU transducer and the US scanner.

4.3 Interaction between the PCD Transducer and the US Scanner

Another interaction to be investigated is between the PCD transducer and the US scanner. Because the time windows of interest overlap, it is important to measure the signal received by the PCD transducer from the US scanner. The interaction was measured by driving the US scanner at different powers at a frequency of 5 MHz.

It can be concluded that there is significant interaction between the 2 sensors. The amount of power received by the PCD transducer directly from the US scanner was 120 % (worst case) of the power received from backscatter of the microbubbles of the pressure wave from the HIFU transducer when both devices are driven at their maximum power. Therefore the output power of the US scanner should be minimized. A disadvantage of a lower output power is the decreased signal to noise ratio (SNR) in the US images. A suitable compromise is to set the output of the US scanner to 5 % of its maximum.

4.4 Other Calibration Measurements

To verify the suitability of the setup, all single parts are tested. The digital camera is evaluated on the quality of the images that are recorded. It is important that the images show details of the kidney stone during an experiment; therefore, the kidney stone should stay in focus. The PCD was tested on its ability of recording signals that contain the backscatter of the HIFU pulse and cavitation events. It should not contain signals caused by interaction. The last part of the setup that was tested is the ACD. The acoustic response of several types of microbubbles was also tested.

The first test experiment was performed to check whether the stone stayed in the focus during HIFU exposure. After enabling the master trigger signal the stone starts to jump in the holder and finally falls out of the holder. To overcome this problem, an acoustically and

optically transparent gel was put in the holder above the stone. Now the stone stays at a fixed position and the camera is able to make clear and bright pictures during HIFU exposure.

The second test experiment should clarify if scattered and cavitation signals can be recorded by means of PCD. The HIFU transducer is driven at its resonance frequency at 50% of its maximum output power. Polymer shelled microbubbles with a mean diameter of 2 μm are infused in the focal region. The signal received by the PCD transducer contains an unwanted signal caused by electromagnetic coupling between transmit and receive section of the setup. The amplitude of this unwanted signal was lowered by connecting every component to a different grounded power socket.

The test on ACD was performed with polylactideacid (PLA) shelled microbubbles. Figure 4.2 shows the image of the US scanner for intensity under the cavitation threshold (A) and above the cavitation threshold (B). Because of the thick shell these bubbles do not scatter US very efficiently. When the bubbles are excited above the cavitation threshold, air diffuses out of the bubbles and free air bubbles are formed. This free air bubbles reflect the US, which explains the bright spots on the image.

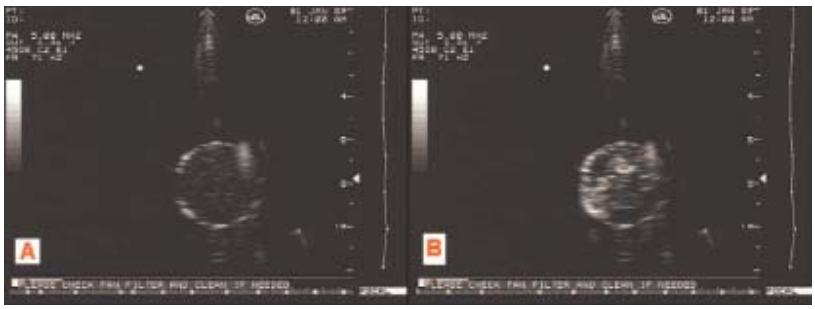

Figure 4.2 Focal region before (a) and after (b) US excitation.

5. RESULTS

The results can be divided into four parts. In section 5.1, optical flow cell measurements are given. In section 5.2, active cavitation detection results are listed. In section 5.3, passive cavitation detection results are given. Finally, in section 5.4, cavitation effects on kidney stones are given.

5.1 Optical Cavitation Detection

Optical cavitation detection was performed to observe how the bubbles behave under ultrasound. When there is no ultrasound activation, the bubbles stay at rest and do not show any oscillating behavior as shown in Figure 5.1. The microbubbles here are unfiltered PLA microbubbles.

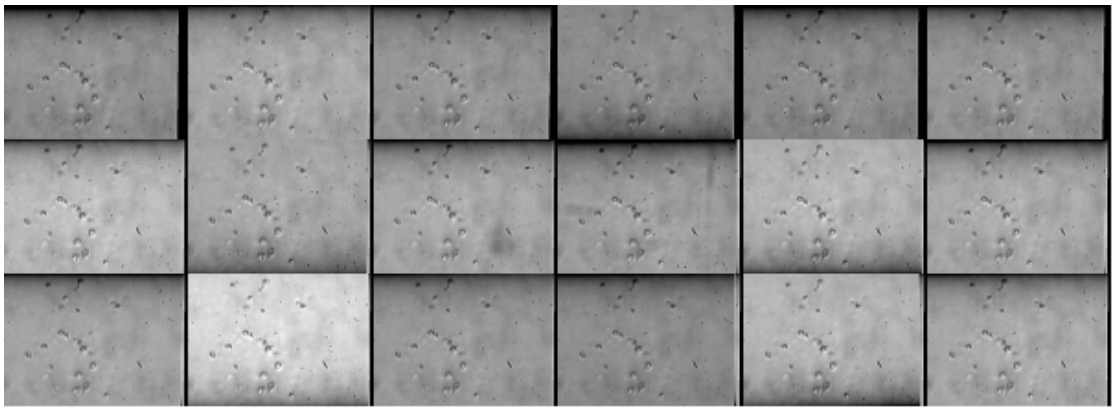

Figure 5.1 PLA microbubbles at rest with no ultrasound excitation.

When these bubbles are excited by ultrasound, they start oscillating and at the end, most of them explode, leaving no microbubbles behind. In Figure 5.2, the microbubbles oscillate under the ultrasonic pressure and in Figure 5.3, all bubbles are exploded and no microbubble is visible anymore.

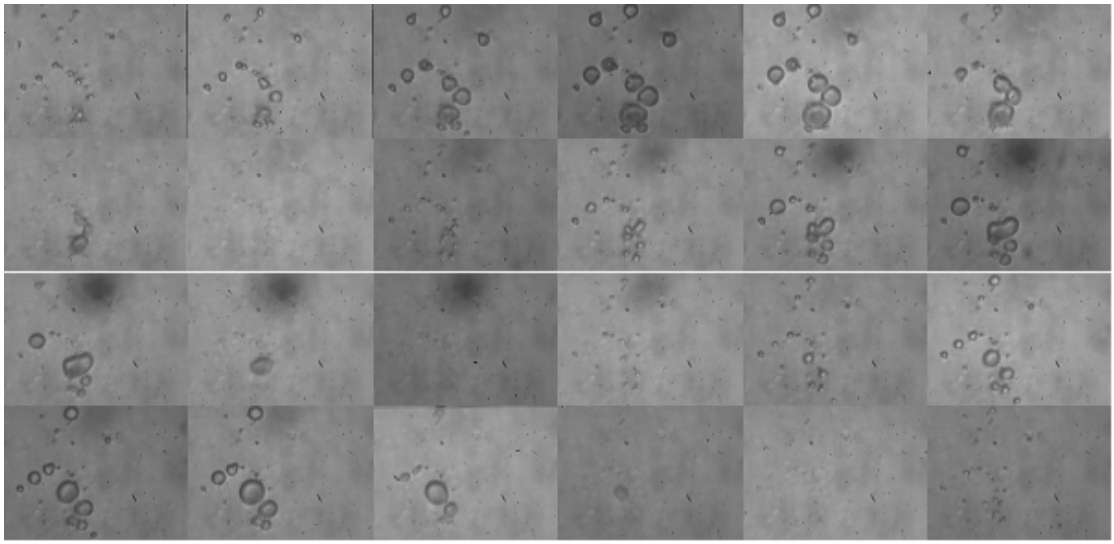

Figure 5.2 PLA microbubbles oscillating under ultrasound excitation.

As can clearly be seen in Figure 5.2, the PLA microbubbles start to oscillate under the ultrasonic pressure. As the ultrasound wave hits the microbubbles, at positive pressures the microbubbles collapse and at negative pressure they expand. In the different snapshots the expansions of the microbubbles are clearly visible.

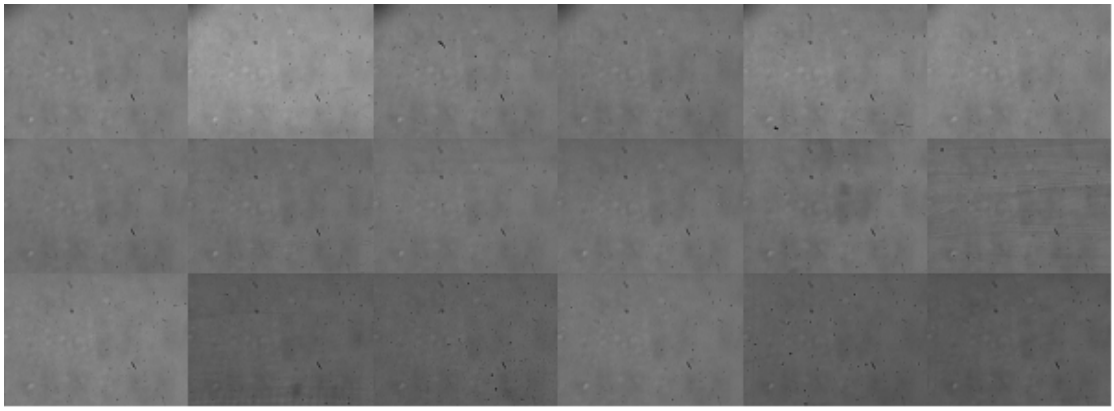

Figure 5.3 PLA – all bubbles have exploded and no bubbles are visible.

This time, the same experiments were performed with a single bubble, which is shown in Figure 5.4 below.

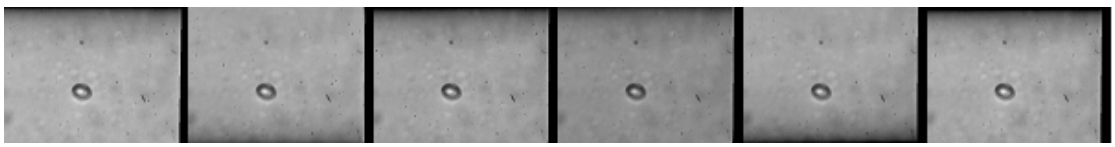

Figure 5.4 PLA microbubbles at rest.

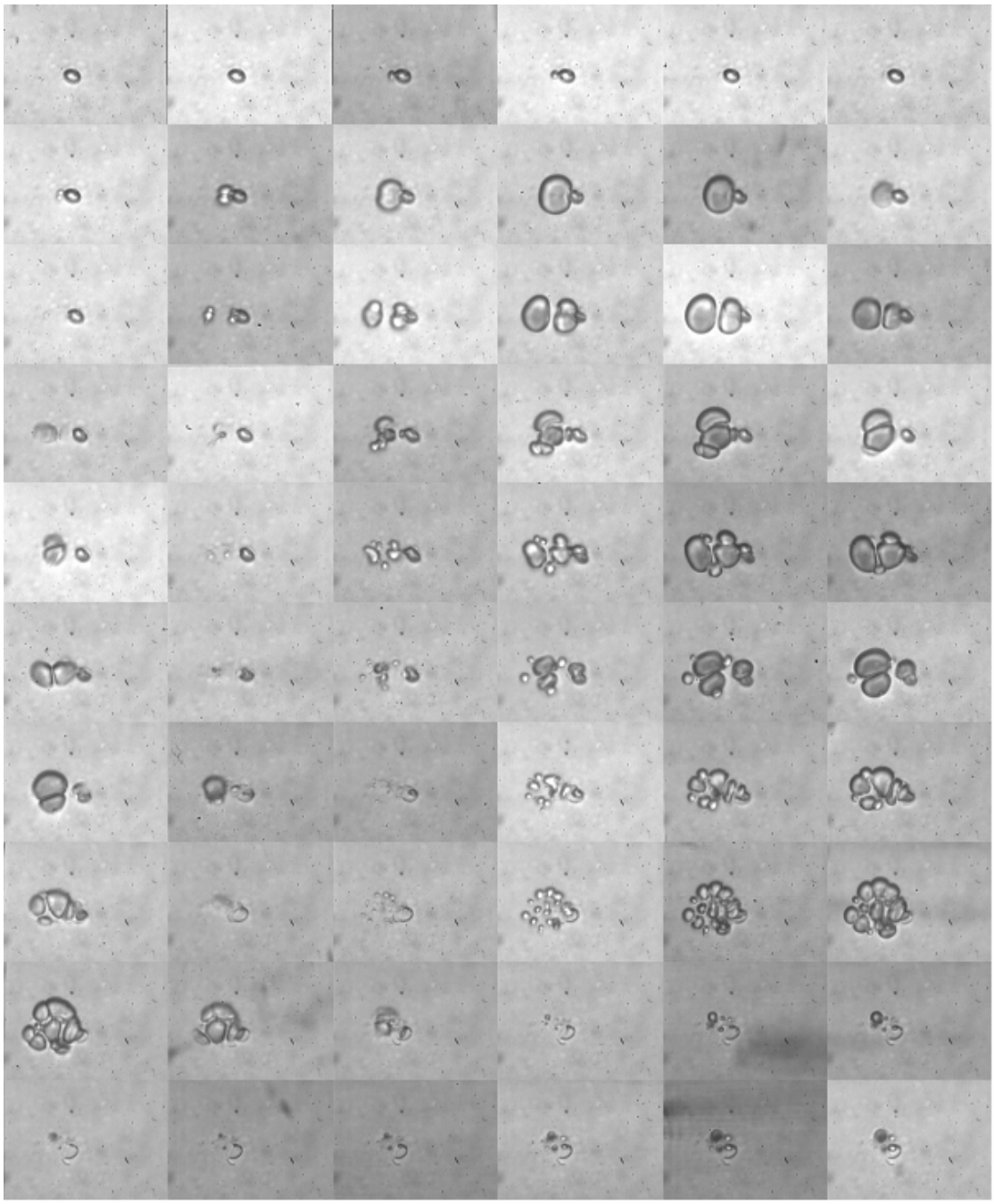

Figure 5.5 Single PLA microbubble oscillating and exploding under ultrasound.

When this single PLA microbubble is exposed to ultrasound, it starts oscillating; during oscillation, it explodes and creates new smaller microbubbles, which also start oscillating immediately, and finally all bubbles explode and release their contents, which is air in this case. Figure 5.5 shows the oscillation of the single microbubble in Figure 5.4.

The same experiments were repeated for a number of times with different amount of PLA microbubbles and similar results were obtained. The general behavior of these PLA microbubbles is as follows: When there is no oscillation, the microbubbles stay intact and do not show any oscillatory behavior. When exposed to ultrasound, depending on the frequency and intensity of the ultrasound, the microbubbles start to oscillate, and at the end eventually explode, releasing their contents. It has been observed that cavitation events take place at low frequencies and high intensities. Under constant frequencies, at low intensities, the microbubbles start to move but do not show a periodic oscillation. As the intensity is increased, the microbubbles start to oscillate, and after a threshold is reached, the bubbles explode and release their contents.

In Figure 5.6, another set of unfiltered PLA microbubbles are seen under no US excitation. When these microbubbles are exposed to US, they start to oscillate and finally collapse as shown in Figure 5.7 below.

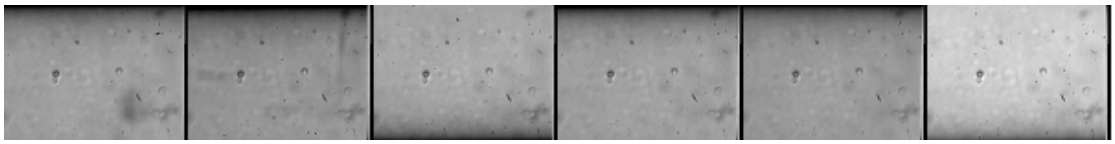

Figure 5.6 PLA microbubbles under no US excitation.

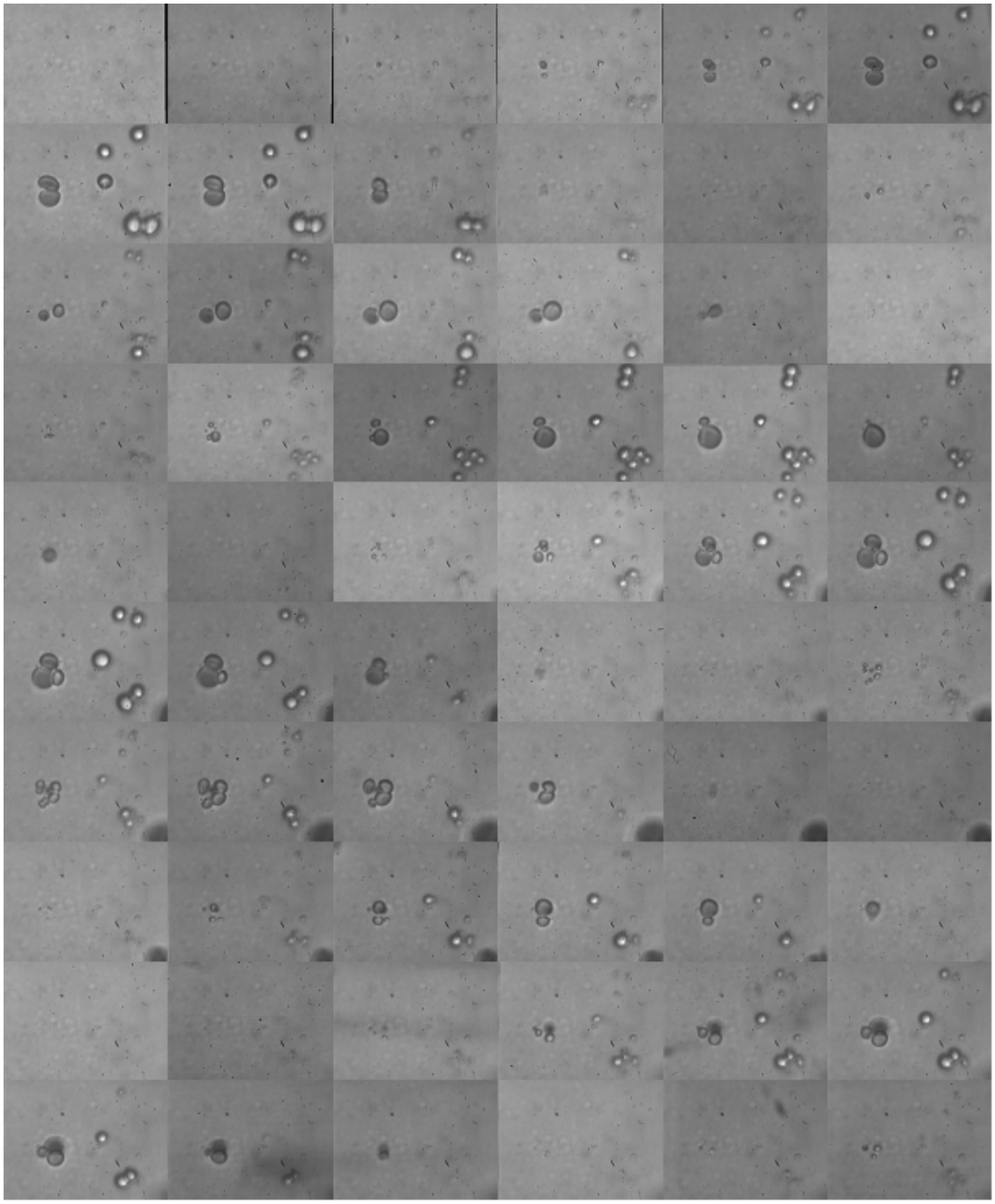

Figure 5.7 PLA microbubbles under US start to oscillate and finally collapse.

5.2 Active Cavitation Detection

Active cavitation detection is performed to observe cavitation events by the help of backscattered signals from the microbubbles. The first tested micro bubble is PLA. Driving the US transducer at 250 mVpp did not generate any cavitation effects in the focal zone of the transducer, which is clearly seen in Figure 5.8.

Figure 5.8 PLA microbubbles excited by an ultrasonic pulse of 250 mVpp.

When the US transducer was driven with an input voltage of 400 mVpp or higher, air bubbles were observed in the focal zone by ACD, which indicates the presence of free gas bubbles due to cavitation of microbubbles. Figure 5.9 shows 6 images of a movie recorded during an experiment of the same PLA microbubbles excited by an ultrasonic pulse of 400 mVpp. The first image is recorded before the ultrasound burst, the following two during the ultrasound excitation, and the rest three images after the US burst. As can clearly be seen, before the ultrasound excitation, there is no visible cavitation events. During the ultrasound excitation, a visible cavitation event takes place on the left side of the balloon, which is still visible in the three images taken after the ultrasound burse is finished. The movement of the microbubbles and the visible whitening of some areas of the balloon where the microbubbles are kept is a clear evidence for the cavitation event.

Figure 5.9 PLA microbubbles excited by an ultrasonic pulse of 400 mVpp.

The same PLA microbubbles were exposed to different intensities of ultrasound burst which is shown in the following figures. In Figure 5.10, microbubbles under an ultrasonic burst of 500 mVpp are displayed.

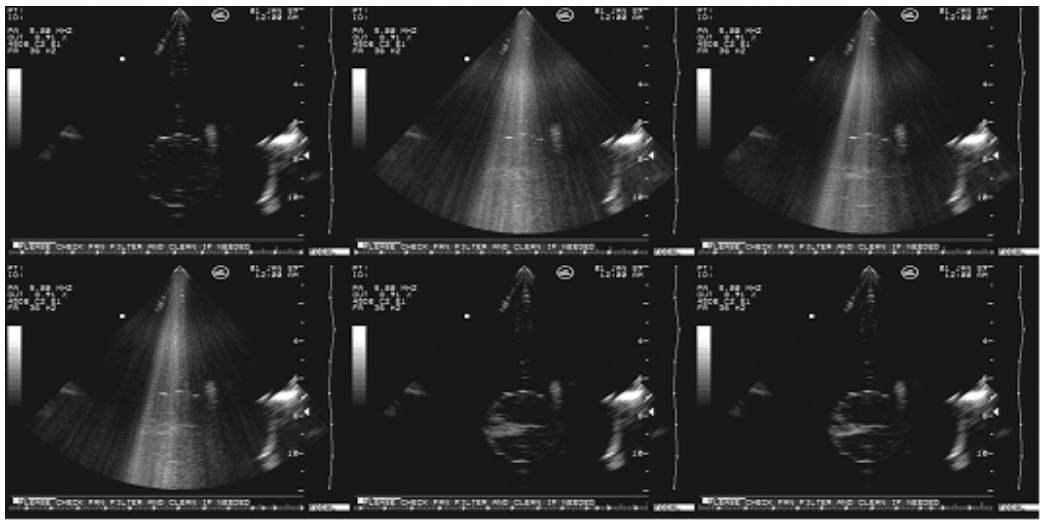

Figure 5.10 PLA microbubbles excited by an ultrasonic pulse of 500 mVpp.

In Figures 5.11 and 5.12, the same microbubbles exposed to an ultrasonic burst of 750 mVpp and 1000 mVpp are displayed, respectively.

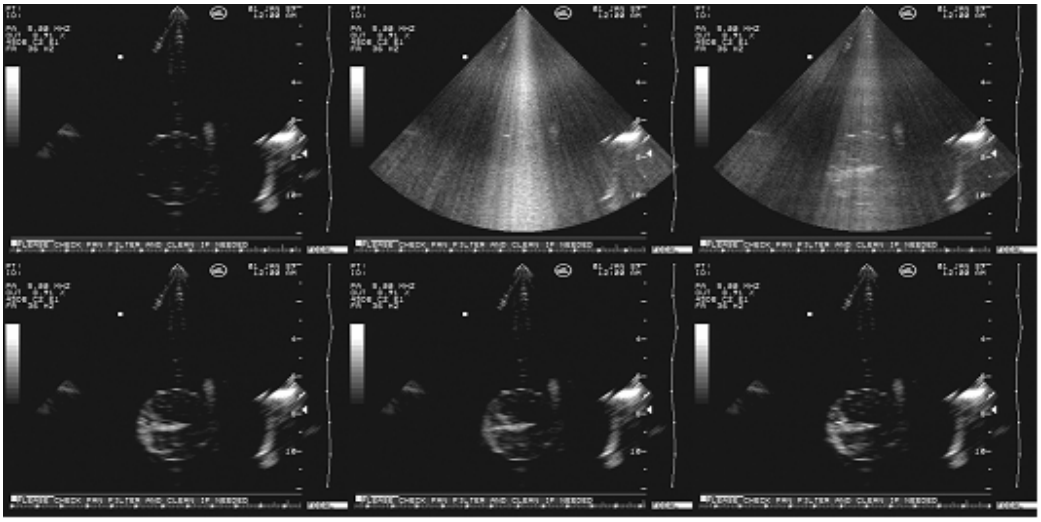

Figure 5.11 PLA microbubbles excited by an ultrasonic pulse of 750 mVpp.

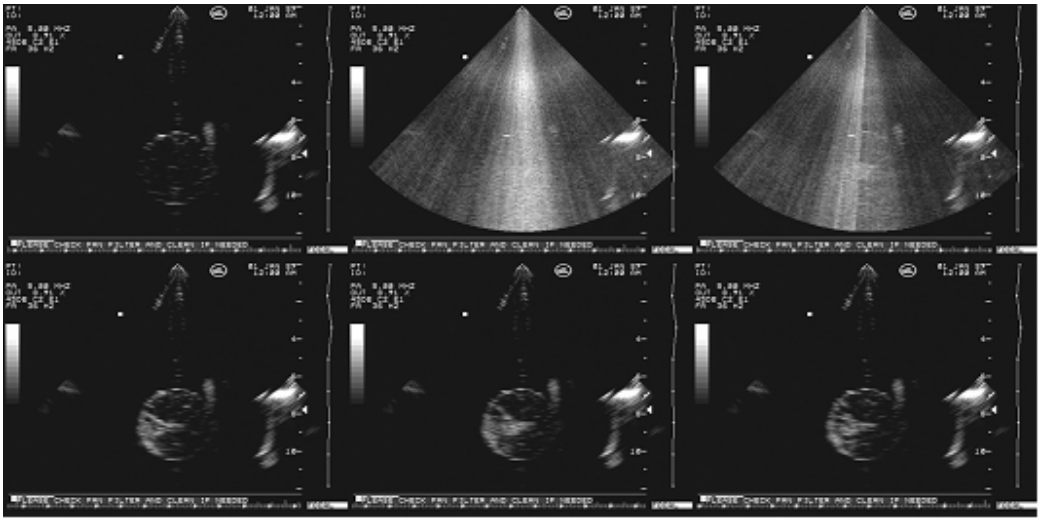

Figure 5.12 PLA microbubbles excited by an ultrasonic pulse of 1000 mVpp.

As can be seen in the figures above, when the microbubbles are exposed to an ultrasonic pulse of 400 mVpp or higher, cavitation events occur and are clearly detected.

The second tested micro bubble is Definity (Bristol Myers Squibb Medical Imaging, Cincinnati, OH, USA). During excitation a dark spot appeared in the focal zone surrounded by some small bright spots, which is visible in Figure 5.13.

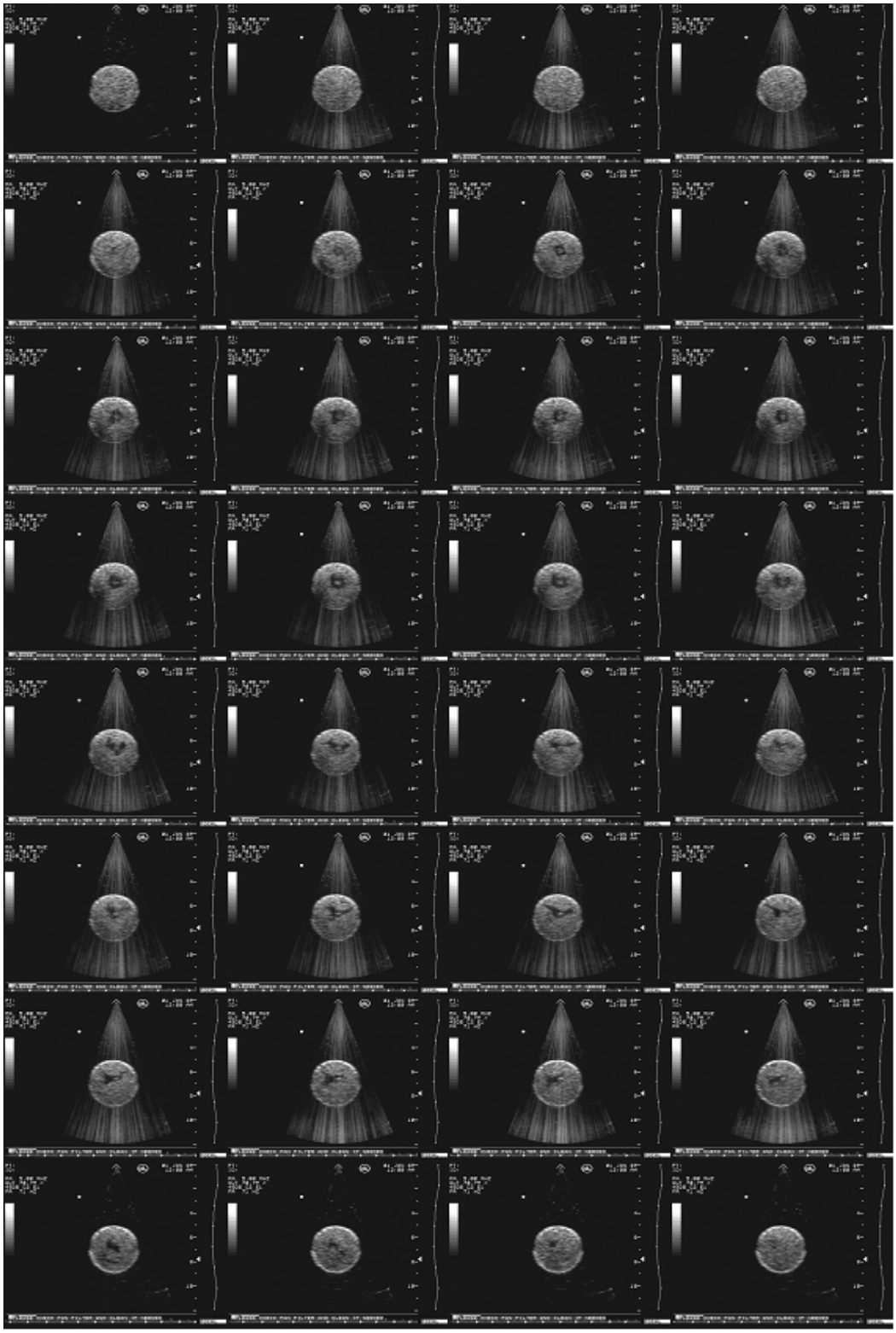

Figure 5.13 Definity under ultrasound excitation.

Finally, the last tested material was polyvinyl-alcohol (PVA), which is a gas holding solution, tested as a cavitation medium. The results obtained with PVA are shown in Figure 5.14.

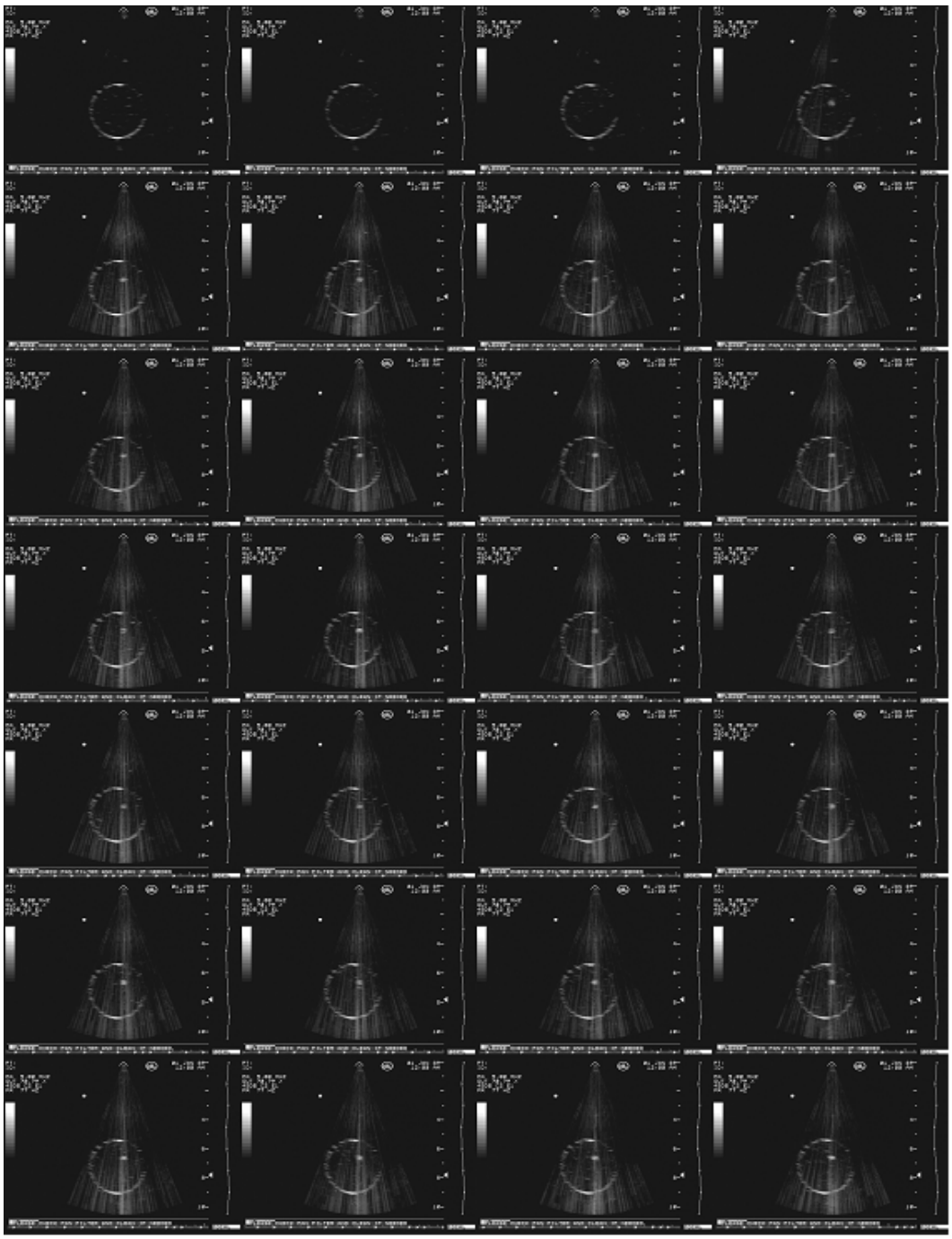

Figure 5.14 PVA under ultrasound excitation.

5.3 Passive Cavitation Detection

Passive cavitation detection was performed with PLA microbubbles in the focal zone. Figure 5.15 shows the frequency spectrum of PLA bubbles generated by a pressure wave. The spectrum is compensated for the frequency response of the US transducer. The fundamental frequency, second, third, and even fourth harmonics due to nonlinear bubble dynamics are clearly visible in the spectrum of the signal. If there were no cavitation events, it is expected to receive only the fundamental frequency on the frequency spectrum of the signals measured from the microbubbles. The presence of these harmonics is a clear evidence for the occurrence of cavitation events.

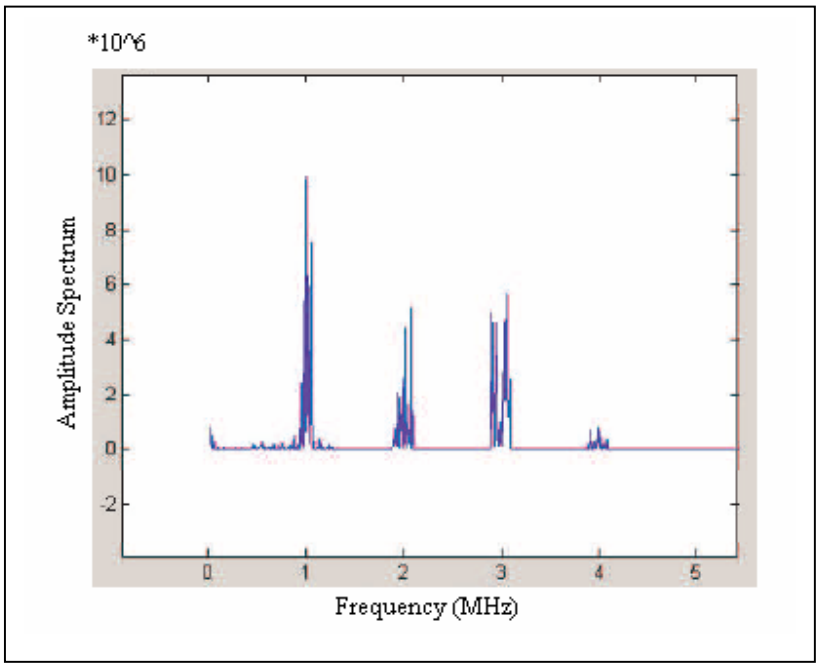

Figure 5.15 Spectrum of cavitating PLA microbubbles.

5.4 Effects on Kidney Stones

The first stones that were tested in the setup are the artificial kidney stones made of Brushite. After 5 minutes of excitation (without micro bubble infusion) at the maximum power

of the HIFU transducer, a pulse length of 100 cycles and PRF of 1 Hz, no visible damage was generated to the kidney stone. After increasing the number of cycles to the maximum that the signal generator supports still no visible damage was observed and no stone weight difference could be estimated. The same experiments were performed with infusion of PLA microbubbles. The results, however, did not change.

The stones of plaster are the second type of stones that were tested. After 5 minutes of excitation with the maximum number of cycles, a small hole was detected in the stone. The weight of the stone was reduced from 1.145 gram to 1.125 gram, which is a weight reduction of 1.75 %. This experiment was repeated twice, resulting in a weight reduction of 1.61 and 1.47 %, respectively. The same experiment was repeated with PLA micro bubbles. Again a small hole was found in the stone after the experiment. The weight reduction was similar (1.83 %) to the experiments without micro bubbles. The repeated experiments resulted in a weight reduction of 1.97 and 1.63 %. Figure 5.16 shows the holes in the stones of the experiments with and without bubbles.

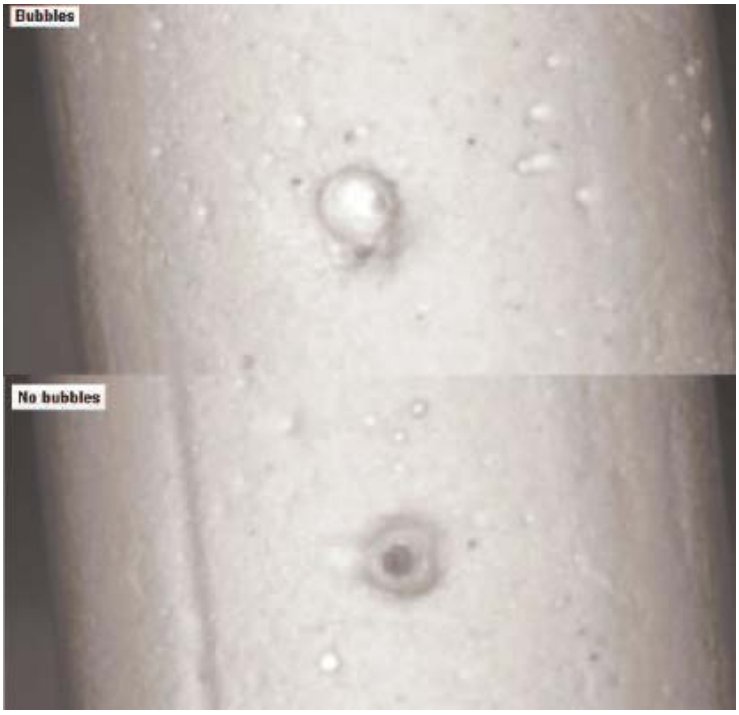

Figure 5.16 Damage of the artificial kidney stones with and without micro bubbles.

6. DISCUSSION

The experiments with the HIFU transducer, driven at its maximum pressure, were performed with PLA, Definity and PVA. Because of the low frame rate of the US scanner, only a high number of cycles showed the generation or collapse of free air bubbles with ACD.

During the active cavitation detection experiments with PLA microbubbles, driving the US transducer at 200 or 300 mVpp did not generate any cavitation effects in the focal zone of the transducer. When the US transducer was driven with an input voltage of 400 mVpp or higher, air bubbles were observed in the focal zone by ACD, which indicates the presence of free gas bubbles due to cavitation of micro bubbles.

During the active cavitation detection experiments with Definity microbubbles, during excitation, a dark spot appeared in the focal zone surrounded by some small bright spots. This might indicate the massive destruction of micro bubbles in combination with the radiation force and the cavitation of free air bubbles. The size of the dark spot and the number of bright spots increase as the number of cycles increases.

No desirable kidney stone destruction was detected. This is due to several reasons. The first possible explanation for this result is that the power of the HIFU transducer is not so high, so that not enough power is transferred from the HIFU to the kidney stone and hence no kidney stone destruction was possible. The second reason might be the quality of the produced microbubbles. The used microbubbles were experimental microbubbles produced during the study and were not very good in providing a good cavitation medium for kidney stone destruction.

7. CONCLUSION

This project concerns design, realization and test of a setup that enables the investigation of the effect of micro bubbles on kidney stone destruction by means of high intensity focused ultrasound (HIFU). This setup is equipped with ACD and PCD to observe cavitation events. Besides that, it is possible to monitor the kidney stone by means of a visualization system. These measurements can be performed simultaneously.

ACD is performed by means of a B-mode ultrasound (US) scanner. Because of the low frame rate of the US scanner ACD is only possible with longer pulse lengths of the HIFU transducer. Triggering the scanner enables the use of shorter pulse lengths, but this demands very critical delay estimation. With longer pulse lengths cavitation events could be detected, recorded and displayed in real-time, although the interaction with the HIFU transducer is visible.

PCD is possible with both long and short pulse lengths. The PCD signal is recorded and can be displayed in real-time. After the experiment the amplitude spectrum is calculated off-line. PCD is limited to a PRF of 5 Hz by the amount of data it can transfer to the PC. Simultaneous use of ACD and PCD is possible, although the interaction between the devices should be taken into account by filtering the PCD signal. During the experiment bright and detailed images can be made of the kidney stone. An optically and acoustic transparent gel is needed to keep the stone at a fixed position. However, this does not decrease the quality of the picture. The movie made by the digital camera can be viewed in real-time and is saved for off-line analysis.

No artificial kidney stone could be destructed during test experiments. The stones of Brushite appeared to be hard to damage with the HIFU transducer. In the stones of plaster a hole could be generated with the size of the focal spot of the HIFU transducer. Infusion of PLA micro bubbles or PVA did not significantly increase the damage to the stone. A HIFU

with a higher acoustic pressure and lower resonance frequency might, however, improve considerably the results. A lower resonance frequency implies a larger focal spot. A larger focal spot generates more cavitation jets at the surface of the stone and this might cause severe damage.

An alternative option might be the use of a dual transducer setup. In this case a HIFU transducer is used to create free gas bubbles out of the infused microbubbles and a lower frequency transducer is used to induce cavitation. The disadvantage is that this option reduces the control of cavitation because the focal spot increases considerably.

APPENDIX A. PROTOCOL FOR PREPARATION OF MICROBUBBLES

A.1 Materials

- PLA
- Dichloromethane
- 20mL Syringe
- 1 μm Glass acrodisk filter
- Cyclodecane
- Hexadecane (optional)
- 0.3 % Polyvinyl-alcohol (PVA) in water
- 20 % Polyethylene-glycol (PEG) in water

A.2 Procedure

1. On an analytical scale, weigh out the amount of solid material to use.
2. In a wide-mouth glass, weigh out the amount of cyclodecane and hexadecane to use on a scale in the chemical hood.
3. Weigh out the amount of dichloromethane to use. Act quickly to avoid evaporation.
4. Add the solids to the wide mouth bottle and cap to avoid evaporation. Make sure the solids are fully dissolved before proceeding.
5. Add 10g of 0.3 % PVA.
6. Emulsify by pressing the solution ten times through a 1μm filter.
7. Add a stir bar to the glass and stir with the glass jar open for at least 1 hour in the fume hood to evaporate the dichloromethane.

8. Centrifuge three times at 3,000 RPM (program 2 on the centrifuge). Cut the tip off a transfer pipette so that it has a wide end and use it to recover the top milky layer between centrifugations and mix with Millipore water.
9. After the last centrifugation, recover the top layer and resuspend in the wide-mouth glass jar with 12.0g of Millipore water.
10. Use a pipette to measure 300 μL of 20 % PEG and mix it well.
11. Split the material evenly, about 3g each, between four labeled plastic containers in preparation for freeze drying.
12. Freeze the sample at -80^{o}C.

REFERENCES

1. Brujan E.A., "The role of cavitation microjets in the therapeutic applications of ultrasound", *Ultrasound in Medicine and Biology*, vol. 30(3), pp. 381-387, 2004.

2. Laborde J.L., Bouyer C., Caltagirone J.P., Crard A.G., "Acoustic cavitation field prediction at low and high frequency ultrasounds," *Ultrasonics*, vol. 36, pp.581-587, 1998.

3. Delacretaz G., Rink K., Pittomvils G., Lafaut J.P., Boving R., "Importance of the implosion of ESWL-induced cavitation bubbles," *Ultrasound in Medicine and Biology*, vol. 21(1), pp. 97-103, 1995.

4. Cathignol D., Tavakkoli J., Birev A., Arefiev A., "Comparison between the effects of cavitation induced by two different pressure-time shock waveform pulses," *IEEE Transactions on UFFC*., vol. 45(3), pp. 788-799, 1998.

5. Bailey M.R., Cleveland R.O., Crum L.A., Evan A.P., Lingeman J.E., McAteer J.A., "Cavitation in shock wave lithotripsy: the clinical role in bubble activity in stone breakage and kidney trauma," *IEEE Proc. on Ultrasonic Symposium*, pp. 724-727, 2003.

6. Zhu S., Cocks F.H., Zhoung P., "The role of stress waves and cavitation in stone comminution in shock wave lithotripsy", *Ultrasound in Medicine and Biology*, vol. 28(5), pp. 661-671, 2002.

7. Delius M., "Minimal static excess pressure minimizes the effect of extracorporeal shock wave on cells and reduces it in gallstones", *Ultrasound in Medicine and Biology*, vol. 23(4), pp. 611-617, 1997.

8. Carnell M.T., Gentry T.P., Emmony D.C., "The generation of negative pressure waves for cavitation studies", *Ultrasonics*, vol. 36, pp. 689-693, 1998.

9. Holland C.K., Roy R.A., Apfel R.E., Crum L.A., "In vitro detection of cavitation induced by a diagnostic ultrasound system", *IEEE Trans. On UFFC*, vol. 39(1), pp. 95-101, 1992.

10. W.S. Chen, A.A. Brayam, T.J. Matula, L.A. Crum, "Inertial cavitation dose and hemolysis produced in vitro witj or without Optison," *Ultrasound in Medicine and Biology*, vol. 29(5), pp. 725-737, 2003.

11. Lifshitz D.A., Williams J.C., Sturtevant B., Evan A.P., McAteer J.A., "Quantification of shock wave cavitation damage in vitro", *Ultrasound in Medicine and Biology*, vol. Vol. 23(3), pp. 461-471, 1997.

12. Niederdrank T., "Experimental investigations of the acoustic backscattering of a single cavitation bubble", *Ultrasonics*, vol. 35(7), pp. 517-523, 1997.

13. Sapoznokov O.A., Bailey M.R., Crum L.A., Miller N.A., Cleveland R.O., "Ultrasound guided localized detection of cavitation during lithotripsy in pig kidney in vivo", *IEEE Proc. on Ultrasonic Symposium*, pp. 1347-1350, 2001.

14. Rabkin B.A., Zderic V., Vaezy S., “Involvement of cavitation in the appearance of hyperechoic regions in ultrasound image visualization of high intensity focused ultrasound therapy: in vivo results”, *IEEE Proc. on Ultrasonic Symposium*, pp. 1469-1472, 2004.

15. Lo M.T., Tsao J., Lin S., “Using the correlation property of subharmonic response as an index of cavitation microbubbles”, *IEEE Proc. on Ultrasonic Symposium*, pp. 1383-1386, 2004.

16. Frinking P.J.A., Bouskaz A., Kirkhorn J., Cate F.J.T., Jong N., “Ultrasound contrast imaging: current and new potential methods”, *Ultrasound in Medicine and Biology*, vol. 26(6), pp. 965-975, 2000.

17. Becher H., Burns P., “Handbook of contrast echocardiography”, New York, Springer, 2000.

18. Feinstein S.B., “The powerful microbubble: from bench to bedside, intravascular to therapeutic delivery system, and beyond”, *American Journal of Physiology*, vol. 287, pp. H450-H457, 2004.

19. Miller D., Song J., “Lithotripter shock waves with cavitation agents produce tumor growth reduction and gene transfer in vivo”, *Ultrasound in Medicine and Biology*, vol. 28(10), pp. 1343-1348, 2002.

20. Tran B.C., Seo J., Hall T.L., Fowlkens J.B., Cain C.A., “Microbubble enhanced cavitation for noninvasive ultrasound surgery”, *IEEE Trans. on UFFC*., vol. 50(10), pp. 1296-1304, 2003.

21. Chen W.S., Brayam A.A., Matula T.J., Crum L.A., Miller M.W., “The impulse length dependence of inertial cavitation dose and hemolysis”, *Ultrasound in Medicine and Biology*, vol. 29(5), pp. 739-748, 2003.

22. Hynynen K., Colucci V., Chung A., Jolesz F., “Noninvasive arterial occlusion using MRI-guided focused ultrasound”, *Ultrasound in Medicine and Biology*, vol. 22(8), pp. 1071-1077, 1996.

23. Sokka S.D., King R., Hynynen H., “MRI-guided gas bubble enhanced ultrasound heating in vivo rabbit thigh”, *Physics in Medicine and Biology*, vol. 48, pp. 223-241, 2003.

24. Christiansen J.P., French B.A., Klibanov A.L., Kaul S., Lindner J.R., “Targeted tissue transfection with ultrasound destruction of plasmid-bearings cationic microbubbles”, *Ultrasound in Medicine and Biology*, vol. 29(12), pp. 1759-1767, 2003.

25. Unger E.C., Porter T.R., Culp W., Matsunaga T., Zutshi R., “Therapeutic applications of lipid-coated microbubbles”, *Advanced Drug Delivery Reviews*, vol. 56, pp. 1291-1314, 2004.

26. Dijkmans P.A., Luffermans L.J.M., Musters R.J.P., van Wamel A., ten Cate F.J., van Gilst W., Visser C.A., de Jong N., Kamp O., “Microbubbles and ultrasound: from diagnosis to therapy”, *European Journal of Echocardiography*, vol. 5(4), pp. 245-256, 2004.

27. Tsutsui J.M., Xie F., Porter T.R., “The use of microbubbles to target drug delivery”, *Cardiovascular Ultrasound*, vol. 2(23), pp. 1-7, 2004.

28. Chomas J.E., Dayton P., Allen J., Morgan K., Ferrera K.W., “Detection procedures of ultrasound contrast agents”, *IEEE Trans. on UFFC*., vol. 48(1), pp. 232-248, 2001.

29. Hynynen K., McDonald N., Vykhodtseva N., Jolesz F.A., "Noninvasive MR imaging guided focal opening of the blood brain barrier in rabbits", *Radiology*, vol. 220, pp. 640-646, 2001.

30. Porter T.R. Xie F., "Ultrasound, microbubbles, and thrombolysis", Progress in Cardiovascular Disease, vol. 44(2), pp. 101-110, 2001.

31. Draper D.O., Castel J.C., Castel D., "Rate of Temperature Increase in Human Muscle During 1 MHz and 3 MHz Continuous Ultrasound", *Journal of Orthopaedic & Sports Physical Therapy,* vol. 22(4), pp. 142-150, 1995.

32. Tacker J.R., Anderson R.U., "Delivery of Antitumor Drug to Bladder Cancer by Use of Phase Transition Liposomes and Hyperthermia", *Journal of Urology,* vol. 127, pp. 1211-1212, 1982.

33. Kennedy J.E., Cranston D., "High intensity focused ultrasound: surgery of the future?", *British Journal of Radiology,* vol. 76(909), pp. 590-599, 2003.

34. Madersbacher S., Marberger M., "High-energy shockwaves and extracorporeal high-intensity focused ultrasound", *Journal of Endourology,* vol. 17(8), pp. 667-672, 2003.

35. Huber P.E., Jenne J.W., Rastert R., "A New Noninvasive Approach in Breast Cancer Therapy Using Magnetic Resonance Imaging-guided Focused Ultrasound Surgery", *American Association for Cancer Research,* vol. 61, pp. 8441-8447, 2001.

36. Barnett S.B., Ziskin M.C., Nyborg W.L., Maeda K., Bang J., 'Current Status of Research on Biophysical Effects of Ultrasound', *Ultrasound in Med. & Biol.*, vol. 20(3), pp. 205-218, 1994.

37. Marmottant P., Hilgenfeldt S., "Controlled vesicle deformation and lysis by single oscillating bubbles", *Nature,* vol. 423(6936), pp. 153-156, 2003.

38. Elder S.A., "Cavitation Microstreaming", *Journal of the Acoustical Society of America,* vol. 31(1), pp. 54-64, 1958.

39. Nyborg W.L., "Ultrasonic Microstreaming and Related Phenomena", *Brit. J. of Cancer,* vol. 45, pp. 156-160, 1982.

40. Rooney J.A., "Hemolysis Near an Ultrasonically Pulsating Gas Bubble", *Science,* vol. 169, pp. 869-871, 1970.

41. Brennen C.E., "*Cavitation and Bubble Dynamics",* Oxford University Press, New York, 1995.

42. May D.J., Allen J.S., Ferrara K.W., "Dynamics and fragmentation of thick-shelled microbubbles", *IEEE Trans. on Ultrasonics Ferroelectrics and Frequency Control,* vol. 49(10), pp. 1400-1410, 2002.

43. Urick R.J., "*Principles of Underwater Sound*", McGraw-Hill Book Company, San Francisco, 1983.

44. Hill C.R., "Ultrasonic Exposure Thresholds for Changes in Cells and Tissues", *Journal of Acoustic Society of America,* vol. 52(2), pp. 667-672, 1971.

45. Apfel R.E., Holland C.K., "Gauging the Likelihood of Cavitation from Short-pulse, Low-duty Cycle Diagnostic Ultrasound", *Ultrasound in Medicine and Biology,* vol.17 (2), pp. 179-185, 1991.

46. Leighton T.G., “Transient excitation of insonated bubbles”, *Ultrasonics,* vol. 27, pp. 50-53, 1989.

47. Allen J.S., Kruse D.E., Dayton P.A., Ferrara K.W., “Effect of coupled oscillations on microbubble behavior”, *Journal of the Acoustical Society of America,* vol. 114(3), pp. 1678-1690, 2003.

48. Soetanto K., Chan M., “Study on the lifetime and attenuation properties of microbubbles coated with carboxylic acid salts”, *Ultrasonics,* vol. 38(10), pp. 969-977, 2000.

49. Sboros V., Moran C.M., Pye S.D., McDicken W.N., “The behavior of individual contrast agent microbubbles”, *Ultrasound in Medicine and Biology,* vol. 29(5), pp. 687-694, 2003.

50. Kvikliene A., Jurkonis R., Ressner M., “Modelling of nonlinear effects and the response of ultrasound contrast micro bubbles: simulation and experiment”, *Ultrasonics*, vol. 42(1–9), pp. 301-307, 2004.

51. Ammi, A. Y., Cleveland, R. O., Mamou, J., Wang, G. I., Bridal, S. L., O’Brien, W. D., “Ultrasonic contrast agent shell rupture detected by inertial cavitation and rebound signals”, *IEEE Transactions on Ultrasonics Ferroelectrics and Frequency Control*, vol. 53(1), pp. 126-136, 2006.

52. Heimbach, D., Munver, R., Zhong, P., Jacobs, J., Hesse, A., Muller, S. C., and Preminger, G. M., “Acoustic and mechanical properties of artificial stones in comparison to natural kidney stones”, *Journal of Urology*, vol. 164(2), pp. 537-544, 2000.

53. Tran, B. C., Seo, J., Hall, T. L., Fowlkes, J. B., and Cain, C. A., “Effects of contrast agent infusion rates on thresholds for tissue damage produced by single exposures of high-intensity ultrasound”, *IEEE Transactions on Ultrasonics Ferroelectrics and Frequency Control*, vol. 52(7), pp. 1121-1130, 2005.

54. Harris, F. J., “Use of Windows for Harmonic-Analysis with Discrete Fourier-Transform”, *Proceedings of the IEEE*, vol. 66(1), pp. 51-83, 1978.

55. Cathignol, E., Tavakkoli, J., Birer, A., Arefiev, A., “Comparison between the effects of cavitation induced by two different pressure time shock waveform pulses”, *IEEE Transactions on Ultrasonics, Ferroelectrics and Frequency Control*, vol. 45(3), pp. 788-799, 1998.

56. Min, J. C., Doh, D., Tae, G. H., Chu, H. C., Dong, G. P., Rim, G., Coleman, A., “Acoustic streaming in lithotripsy fields: preliminary observation using a particle image velocimetry method”, *Ultrasonics,* vol. 44(2), pp. 133-145, 2006.